

A Stiction Oscillator with Canards: On Piecewise Smooth Nonuniqueness and Its Resolution by Regularization Using Geometric Singular Perturbation Theory*

Elena Bossolini[†]
Morten Brøns[†]
Kristian Uldall Kristiansen[†]

Abstract. In mechanics, one often describes microscopic processes such as those leading to friction between relative interfaces using macroscopic variables (relative velocity, temperature, etc.) in order to avoid models of intangible complexity. As a consequence, such macroscopic models are frequently nonsmooth, a prominent example being the Coulomb law of friction. In many cases, these models are perfectly adequate for engineering purposes. Formally, however, since the Fundamental Theorem of Existence and Uniqueness does not apply to these situations, one generally expects that these models possess forward nonuniqueness of solutions. Consequently, numerical computations of such systems might possibly unknowingly discard certain solutions. In this paper, we try to shed further light on this issue by studying solutions of a simple friction oscillator subject to *stiction* friction. The stiction law is a simple nonsmooth model of friction that is a modification of Coulomb based on the fundamental observation that the *dynamic* friction force, when the mass is in motion, is smaller than the *static* friction force during *stick*. The resulting piecewise smooth vector field of this discontinuous model does not follow the classical Filippov convention, and the concept of a Filippov solution cannot be used. Furthermore, some Carathéodory solutions, i.e., absolutely continuous solutions satisfying the differential equation in a weaker sense, are nonphysical. Therefore, we introduce the concept of stiction solutions. These are the Carathéodory solutions that are physically relevant, i.e., the ones that follow the stiction law. However, we find that some of the stiction solutions are forward nonunique in subregions of the slip onset. We call these solutions singular, in contrast to the regular stiction solutions that are forward unique. In order to further understanding of the nonunique dynamics, we then introduce a general regularization of the model. This gives a singularly perturbed problem that captures the main features of the original discontinuous problem. Using geometric singular perturbation theory, we identify a repelling slow manifold that separates the forward slipping from the forward sticking solutions, leading to high sensitivity to the initial conditions. On this slow manifold we find canard trajectories that have the physical interpretation of delaying the slip onset. Most interestingly, we find that these new solutions do not correspond to *stiction solutions* in the piecewise-smooth limit, and are therefore seemingly *nonphysical*, yet they are robust and appear generically in the class of regularizations we consider. Finally, we show that the regularized problem has a family of periodic orbits interacting with the canards. We observe that this family has a saddle stability and that it connects, in the rigid body limit, the two regular, slip-stick branches of the discontinuous problem, which are otherwise disconnected.

Key words. stiction, friction oscillator, non-Filippov, regularization, canard, slip-stick, delayed slip onset

*Published electronically November 3, 2020. This paper originally appeared in *SIAM Journal on Applied Dynamical Systems*, Volume 16, Number 4, 2017, pages 2233–2258, under the title “Canards in Stiction: On Solutions of a Friction Oscillator by Regularization.”

<https://doi.org/10.1137/20M1348273>

[†]Department of Applied Mathematics and Computer Science, Technical University of Denmark, Kongens Lyngby 2800, Denmark (elena.bossolini@icloud.com, mobr@dtu.dk, krkri@dtu.dk).

AMS subject classifications. 34A36, 34E15, 34C25, 37N15, 70E18, 70E20

DOI. 10.1137/20M1348273

Contents

1 Introduction	870
2 Model	871
3 Geometric Analysis of the Discontinuous System	874
4 Forward Solutions of the Discontinuous System	876
5 Regularization	878
6 Slip-Stick Periodic Orbits	887
6.1 Slip-Stick Periodic Orbits in the Regularized System	889
7 Conclusions	893
References	894

1. Introduction. Friction is a tangential reaction force that appears whenever two rough surfaces are in contact. This energy-dissipating force is desirable in car brakes [6], it occurs at the boundaries of the Earth's crustal plates during fault slip [47, 68], and it causes the sound of string instruments [1, 16]. Friction may initiate undesirable noise, like the squeaking of chalk on a blackboard or the squealing of train wheels on tight curves [24]. It may also induce chattering vibrations, as in machine tools [53] and in relay feedback systems [49].

The variety of the abovementioned examples underlines the importance of understanding the friction force, although this is far from being accomplished. For instance, little is known on the shape of the friction law for small velocities, as it is difficult to verify it experimentally [25, 55]. However, it is recognized that the maximal value of the friction force at *stick*, that is, at zero relative velocity, is higher than at *slip*, when the two surfaces are in relative motion [56]. Several models of friction exist in the literature [50, 51, 67, 68], some of them smooth (yet singularly perturbed) like the *rate-and-state models* [13, 14, 55, 57]; see [4, 39, 54] for recent mathematical analysis of such models. Nevertheless, the simplest models are frequently only piecewise smooth, being discontinuous at stick, like the stiction model. Stiction defines a maximum *static* friction force during stick and a lower *dynamic* friction force at slip. In subsets of the discontinuity, the stiction model has solutions that are forward nonunique. In these subsets, a numerical simulation, for example, requires a choice of forward integration, possibly discarding solutions.

A very classical way to resolve nonuniqueness that is outside the scope of discontinuous differential equations (see, e.g., [58, 63]) is to perform a regularization by replacing the ill-posed system with a “nearby,” in some appropriate sense, well-posed system (or even a family hereof). This area of research has recently been very active within the field of piecewise-smooth systems [27, 29, 30, 35, 36, 37, 38, 40, 45]. Here, a regularization is achieved by smoothing out the discontinuity set. The refer-

ences [36, 40] (see also [45]) have developed a geometric approach to studying such systems based upon a combination of an adaptation of the blowup technique [15, 41] and geometric singular perturbation theory (GSPT) [17, 18, 31, 61]. This approach enables a geometric matching between the *area of smoothing* and the region outside using only classical hyperbolic methods of dynamical systems theory [46], and it has proved successful in the description of many nonsmooth phenomena that are closely related to nonuniqueness: nonsmooth bifurcations of limit cycles in a friction oscillator (see [30, 40]) and nonclassical relaxation oscillations in cell biology and in electrical engineering (see [29, 32, 38]).

This paper aims to unveil, through mathematical analysis, new features of the stiction law relating to nonuniqueness; more specifically, the *slip onset*, i.e., when the surfaces start to slip. The paper shows that, in certain circumstances, the slip onset is delayed with respect to the instant that the external forces have equaled the maximum static friction. This result, which in principle could be tested experimentally, has physical implications that may further the understanding of phenomena related to friction.

The paper studies these new features of the stiction law in a model of a friction oscillator subject to stiction [59]. This is a discontinuous system, and one might be tempted to study it using the well-developed theory of Filippov (see [12, 19]). However, the model's vector field is not obtained from a linear convex combination of two adjacent equations on the discontinuity set, and for this reason we say that our model is non-Filippov. New concepts of solutions of a discontinuous system are introduced: *singular/regular stiction solutions* on the basis of the physics of the model. Specifically, the singular stiction solutions lack forward uniqueness in certain subregions of the slip onset. Here it is not possible to predict whether the oscillator will slip or stick in forward time. To deal with the nonuniqueness, a regularization is introduced [35, 60]: this gives a smooth, singularly perturbed problem that captures the main features of the original problem. Using GSPT, we show that the lack of uniqueness turns into a high sensitivity to the initial conditions of the regularized system, where a repelling slow manifold separates sticking from slipping solutions. Along this manifold, canard-like trajectories appear. These canard trajectories are the trajectories that delay the slip onset. We show that these new solutions are not *stiction solutions* and are therefore seemingly *nonphysical*, yet they are robust, appearing generically in any regularization.

It is already known that the friction oscillator may exhibit chaotic [26, 44] and periodic behavior [9, 49, 52]. The paper shows, with a numerical computation, that there exists a family of slip-stick periodic orbits interacting with the canard solutions. This family connects, at the rigid body limit, the two branches of slip-stick orbits of the discontinuous problem. Furthermore, we prove that the orbits of this family are highly unstable, due to a folded saddle and a “canard explosion” of the Floquet multipliers.

The paper is structured as follows. Section 2 presents the model, and section 3 studies its geometrical structure. Section 4 introduces a concept of solution that makes sense for the discontinuous model, and section 5 introduces the regularization. Section 6 shows slip-stick periodic orbits interacting with the canard solutions. Finally, section 7 concludes the paper and discusses the results.

2. Model. A friction oscillator consists of a mass M that sits on a rough table, as shown in Figure 1, and that is subject to a periodic forcing $F_\omega(\bar{t}) := -A \sin(\omega\bar{t})$ with A and ω parameters and \bar{t} time. The mass is connected to a spring of stiffness κ that

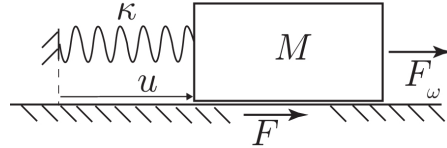


Fig. 1 Model of a friction oscillator.

at rest has zero length. Hence, the spring elongation u corresponds to the position of M . In addition, the motion of the mass on the rough table generates a frictional force F that aims to oppose this movement. The system of equations describing the friction oscillator is

$$(1) \quad \begin{aligned} \dot{u} &= v, \\ M\dot{v} &= -\kappa u + F_\omega(\bar{t}) + F. \end{aligned}$$

The friction force F is modeled as stiction. According to this law, F has different values depending on whether or not the slip velocity v is zero. During slip ($v \neq 0$), stiction is identical to the classical Coulomb law: the friction force is constant and acts in the opposite direction to the relative motion,

$$(2) \quad F = -Nf_d \operatorname{sign} v \quad \text{when } v \neq 0.$$

In (2) the parameter N is the normal force, f_d is the dimensionless dynamic friction coefficient, and the sign function is defined as

$$\operatorname{sign} \alpha := \begin{cases} 1 & \text{if } \alpha > 0, \\ -1 & \text{if } \alpha < 0. \end{cases}$$

Figure 2(a) illustrates the slipping law (2). For zero slip velocity ($v = 0$), it is necessary to consider whether this happens over a time interval or instantaneously, i.e., whether or not \dot{v} is also zero. The former case ($v = \dot{v} = 0$) defines the stick phase, and from (1) it follows that

$$(3) \quad F = w(\bar{t}, u) \quad \text{when } v = 0 \quad \text{and} \quad |w| < Nf_s,$$

where $w(\bar{t}, u) := \kappa u - F_\omega(\bar{t})$ is the sum of forces that induce the motion of M . The parameter f_s in (3) is the dimensionless static friction coefficient, and $f_s > f_d > 0$ [56]. The idea is that the value of the static friction is exactly the value that counteracts the other forces acting on M , so that the mass will keep on sticking. However, the static friction (3) can only oppose the motion of M up to the maximum static friction $\pm Nf_s$, and thus

$$F = Nf_s \operatorname{sign} w \quad \text{when } v = 0 \quad \text{and} \quad |w| > Nf_s.$$

In this latter case the friction force is not sufficient to maintain $\dot{v} = 0$, and therefore the mass will slip in forward time. Figure 2(b) illustrates the friction law for $v = 0$. In compact form, stiction is written as

$$F(v, w) = \begin{cases} -Nf_d \operatorname{sign} v, & v \neq 0, \\ w, & v = 0 \text{ and } |w| < Nf_s, \\ Nf_s \operatorname{sign} w, & v = 0 \text{ and } |w| > Nf_s. \end{cases}$$

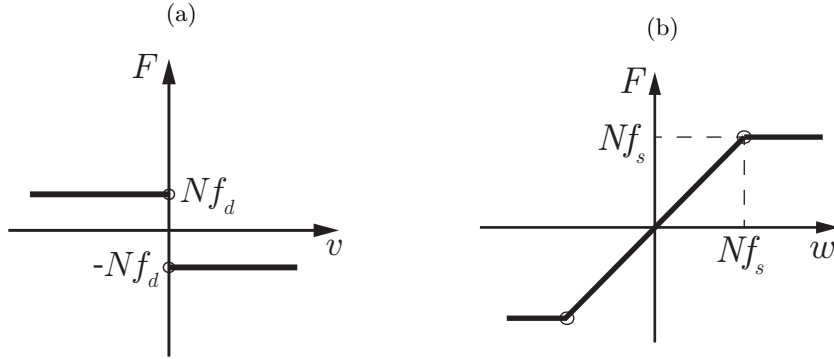


Fig. 2 Stiction friction $F(v, w)$. (a) $v \neq 0$. (b) $v = 0$.

The friction law is not defined for $v = 0$ and $|w| = Nf_s$, where the external forces equal the maximum static friction during stick. Other modeling choices may fix a value of F in these points. These choices do not affect the results of the following analysis; see section 4. By rescaling

$$u = \frac{V}{\omega}x, \quad v = Vy, \quad \bar{t} = \frac{t}{\omega},$$

system (1) is rewritten in its dimensionless form

$$(4) \quad \begin{aligned} x' &= y, \\ y' &= -\xi(x, \theta) + \mu(y, \xi(x, \theta)), \\ \theta' &= 1, \end{aligned}$$

where $\theta \in \mathbb{T}^1$ is a new variable describing the phase of the periodic forcing, and this makes system (4) autonomous. In this new system the prime has the meaning of differentiation with respect to the time t , and $\gamma := \Omega/\omega$ is the ratio between the natural frequency of the spring $\Omega := \sqrt{\kappa/M}$ and the forcing frequency ω . Therefore, $\gamma \rightarrow \infty$ corresponds to the rigid body limit. Furthermore, in (4) we have introduced the function

$$\xi(x, \theta) := \frac{w}{A} = \gamma^2 x + \sin \theta.$$

Remark 2.1. The function $\xi(x, \theta)$ is the sum of the rescaled external forces. In what follows, we drop the function's arguments when they are unnecessary and simply refer to it as ξ . In some plots (like in Figure 3) we will replace x by $\xi(x, \theta)$ to obtain better pictures.

In (4), the function μ describes the dimensionless stiction law

$$(5) \quad \mu(y, \xi(x, \theta)) = \begin{cases} -\mu_d \operatorname{sign} y, & y \neq 0, \\ \xi, & y = 0 \text{ and } |\xi| < \mu_s, \\ \mu_s \operatorname{sign} \xi, & y = 0 \text{ and } |\xi| > \mu_s, \end{cases}$$

where $\mu_{d,s} := Nf_{d,s}/A$. System (4) together with the friction function (5) is the model used in the rest of the analysis. In compact form it is written as $z' = Z(z)$,

where $z := (x, y, \theta) \in \mathbb{R}^2 \times \mathbb{T}^1$ and $\mathbb{T}^1 := \mathbb{R}/2\pi\mathbb{Z}$. The vector field $Z(z)$ is not defined on the two lines $\{y = 0, \xi = \pm\mu_s\}$. Section 3 studies the phase space of (4) using geometrical tools from piecewise-smooth theory [12, 19].

3. Geometric Analysis of the Discontinuous System. This section analyzes the friction oscillator (4) with stiction friction (5) in the context of piecewise-smooth dynamical systems. The notation is consistent with that in [21]. System (4) is smooth in the two regions

$$\begin{aligned} G^+ &:= \{(x, y, \theta) \in \mathbb{R}^2 \times \mathbb{T}^1 \mid y > 0\}, \\ G^- &:= \{(x, y, \theta) \in \mathbb{R}^2 \times \mathbb{T}^1 \mid y < 0\}. \end{aligned}$$

Let $Z^+(z)$ ($Z^-(z)$) be the vector field $Z(z)$ restricted to G^+ (G^-) and extended to the closure of G^+ (G^- , respectively). These two smooth vector fields have the explicit form

$$Z^\pm = \begin{cases} x' = y, \\ y' = -\xi(x, \theta) \mp \mu_d, \\ \theta' = 1. \end{cases}$$

The set $\Sigma := \{(x, y, \theta) \in \mathbb{R}^2 \times \mathbb{T}^1 \mid y = 0\}$ is a surface of discontinuity of $Z(z)$ called the *switching manifold*. The vector field $Z(z)$ is well defined in $\Sigma \setminus \{\xi = \pm\mu_s\}$, and its dynamics on the y -coordinate is

$$y' = -\xi(x, \theta) + \mu(0, \xi(x, \theta)) \begin{cases} > 0 & \text{for } \xi < -\mu_s, \\ = 0 & \text{for } |\xi| < \mu_s, \\ < 0 & \text{for } \xi > \mu_s. \end{cases}$$

Therefore, it is natural to subdivide Σ into the three sets

$$\begin{aligned} \Sigma_c^+ &:= \{(x, y, \theta) \in \mathbb{R}^2 \times \mathbb{T}^1 \mid y = 0 \text{ and } \xi < -\mu_s\}, \\ \Sigma_s &:= \{(x, y, \theta) \in \mathbb{R}^2 \times \mathbb{T}^1 \mid y = 0 \text{ and } -\mu_s < \xi < \mu_s\}, \\ \Sigma_c^- &:= \{(x, y, \theta) \in \mathbb{R}^2 \times \mathbb{T}^1 \mid y = 0 \text{ and } \xi > \mu_s\} \end{aligned}$$

that are shown in Figure 3(a). The set Σ_c^+ (Σ_c^-) is called the *crossing region pointing upwards* (*downwards*) because orbits here switch from G^- to G^+ (from G^+ to G^-). The strip Σ_s is called the *sticking region* because trajectories within it are not allowed to switch to G^\pm , and they correspond to solutions where the mass sticks to the table. Let $Z_s(z)$ be the vector field $Z(z)$ restricted to Σ_s and extended to the closure of Σ_s . This two-dimensional vector field has the explicit form $(x, \theta)' = (0, 1)$, and thus Σ_s is foliated by invariant arcs of circles

$$(6) \quad \mathcal{F}_{x_0} := \{(x, y, \theta) \in \Sigma_s \mid x = x_0\},$$

since $\theta \in \mathbb{T}^1$. Figure 3(b) shows the foliation \mathcal{F}_{x_0} . The boundaries of Σ_s with Σ_c^\pm define the two sets

$$\begin{aligned} \partial\Sigma_c^+ &:= \{(x, y, \theta) \in \mathbb{R}^2 \times \mathbb{T}^1 \mid y = 0 \text{ and } \xi = -\mu_s\}, \\ \partial\Sigma_c^- &:= \{(x, y, \theta) \in \mathbb{R}^2 \times \mathbb{T}^1 \mid y = 0 \text{ and } \xi = \mu_s\}. \end{aligned}$$

The vector field $Z(z)$ is not defined on $\partial\Sigma_c^\pm$, but the three vector fields $Z_s(z)$ and $Z^\pm(z)$ are. Indeed, $\partial\Sigma_c^\pm$ belong to the closure of both Σ_s and G^\pm . Hence, on $\partial\Sigma_c^\pm$, solutions may be forward nonunique. This will be discussed in section 4.

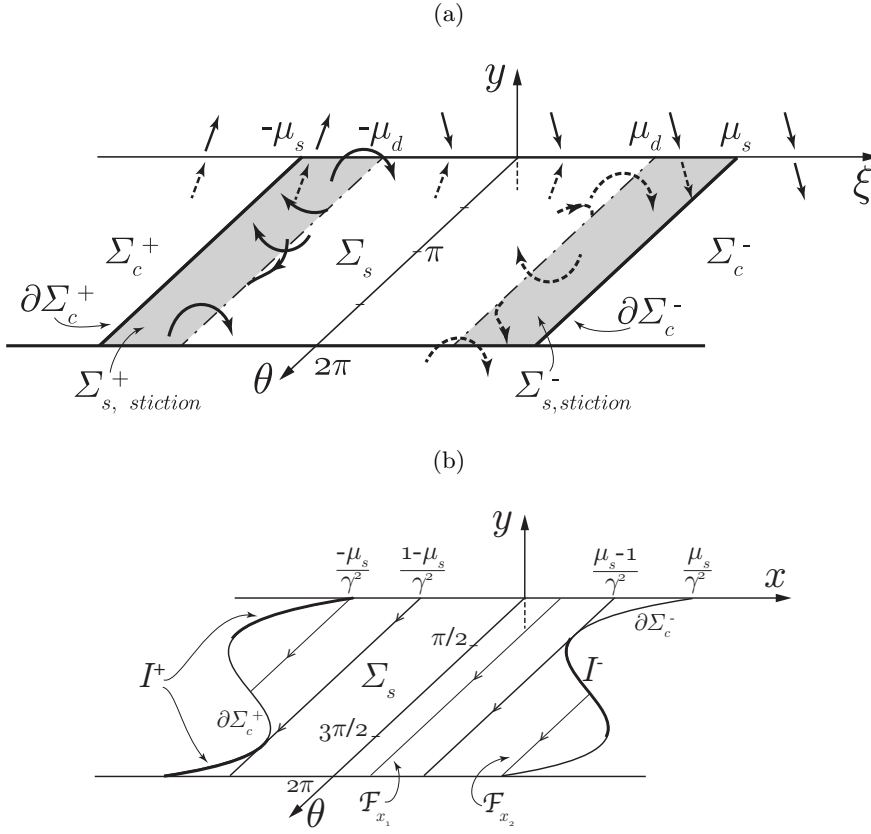


Fig. 3 (a) Vector fields Z^\pm and their tangencies at $\xi = \mp\mu_d$ in the $(\xi(x, \theta), y, \theta)$ -space. Z^- is dashed because it is below Σ_s . The gray bands indicate where Z^\pm suggest crossing, but instead the solution for $y = 0$ is sticking. (b) Phase space of Z_s in the (x, y, θ) -space with the tangencies at $\theta = \{\pi/2, 3\pi/2\}$. The leaf F_{x_1} is a full circle, while F_{x_2} is an arc of a circle. The intervals of nonuniqueness I^\pm are introduced in Proposition 4.4.

Propositions 3.2 and 3.4 below lay out where the vector fields $Z_s(z)$, $Z^\pm(z)$ are tangent to $\partial\Sigma_c^\pm$ and Σ , respectively. The results are shown in Figure 3. First, a definition introduces the concepts of visible and invisible tangency.

DEFINITION 3.1. Let $\hat{\Sigma} := \{z \in \mathbb{R}^n \mid \chi(z) > 0\}$, where $\chi : \mathbb{R}^n \rightarrow \mathbb{R}$ is a smooth and regular function such that $\nabla\chi(z) \neq 0$ for every $z \in \mathbb{R}^n$. Furthermore, let $\hat{Z} : \hat{\Sigma} \rightarrow \mathbb{R}^n$ be a smooth vector field with a smooth extension to the boundary of $\hat{\Sigma}$, that is, for $\chi(z) = 0$. In addition, let $\mathcal{L}_{\hat{Z}}\chi(z) := \nabla\chi \cdot \hat{Z}(z)$ denote the Lie derivative of χ with respect to $\hat{Z}(z)$.

The vector field $\hat{Z}(z)$ is tangent to the set $\chi(z) = 0$ at $p \in \hat{\Sigma}$ if $\mathcal{L}_{\hat{Z}}\chi(p) = 0$. The tangency is called visible (invisible) if $\mathcal{L}_{\hat{Z}}^2\chi(p) > 0$ ($\mathcal{L}_{\hat{Z}}^2\chi(p) < 0$), where $\mathcal{L}_{\hat{Z}}^2\chi(p)$ is the second-order Lie derivative. The tangency is a cusp if $\mathcal{L}_{\hat{Z}}^2\chi(p) = 0$ but $\mathcal{L}_{\hat{Z}}^3\chi(p) \neq 0$.

In other words, the tangency is visible if the orbit $z' = \hat{Z}(z)$ starting at p stays in $\hat{\Sigma}$ for all sufficiently small $|t| > 0$, and it is invisible if it never does so [12, pp. 93 and 237]. A quadratic tangency is also called a *fold* [64].

PROPOSITION 3.2. *$Z_s(z)$ is tangent to $\partial\Sigma_c^-$ ($\partial\Sigma_c^+$) at the isolated points $\theta \in \{\pi/2, 3\pi/2\}$. The tangency is visible (invisible) for $\theta = \pi/2$ and invisible (visible) for $\theta = 3\pi/2$.*

Proof. Define the function $\chi(x, \theta) = \mu_s - \xi(x, \theta)$ so that it is defined within Σ and its zeros belong to $\partial\Sigma_c^-$. Then $\mathcal{L}_{Z_s}\chi(p) = 0$ in $\theta = \{\pi/2, 3\pi/2\}$. Moreover, $\mathcal{L}_{Z_s}^2\chi(p) = \sin\theta$. Hence, $\theta = \pi/2$ ($\theta = 3\pi/2$) is a visible (invisible) fold. Similar computations prove the result for $\partial\Sigma_c^+$. \square

COROLLARY 3.3. *If $\mu_s > 1$, then the invariant leaves \mathcal{F}_x of (6) with $|\gamma^2 x| < \mu_s - 1$ are periodic orbits with period 2π . The remaining leaves of (6), having $|\gamma^2 x| \geq \mu_s - 1$, escape Σ_s in finite time. If $\mu_s < 1$, no periodic orbits exist on Σ_s .*

Proof. The sticking trajectory $\gamma^2 x(t) = \mu_s - 1$ ($\gamma^2 x(t) = -\mu_s + 1$) is tangent to $\partial\Sigma_c^-$ ($\partial\Sigma_c^+$) because $\xi(x, \pi/2) = \mu_s$ ($\xi(x, 3\pi/2) = -\mu_s$). These two lines coincide for $\mu_s = 1$. When $\mu_s > 1$ the orbits $|\gamma^2 x(t)| < \mu_s - 1$ are included within the two tangent orbits. Hence, they never intersect the boundaries $\partial\Sigma_c^\pm$ and therefore are periodic with period 2π . Instead, the trajectories $\mu_s > |\gamma^2 x(t)| \geq \mu_s - 1$ exit Σ_s in finite time. \square

The orbit $\mathcal{F}_{x_1} \subset \Sigma_s$ of Figure 3(b) is periodic, while \mathcal{F}_{x_2} leaves Σ_s in finite time. The period $T = 2\pi$ corresponds to a period $\bar{T} = 2\pi/\omega$ in the original time \bar{t} , as is often mentioned in the literature [9, 59]. The condition $\mu_s > 1$ corresponds to $Nf_s > A$; that is, the maximum static friction force is larger than the amplitude of the forcing F_ω . This interpretation makes it an obvious condition for having sticking solutions.

PROPOSITION 3.4. *The vector field Z^- (Z^+) is tangent to Σ on the line $\xi = \mu_d$ ($\xi = -\mu_d$). The tangency is invisible (visible) for $\theta \in [\pi/2, 3\pi/2[$, and it is visible (invisible) for $\theta \in [0, \pi/2[$ and $\theta \in]3\pi/2, 2\pi[$, while it is a cusp on the isolated points $\theta = \{\pi/2, 3\pi/2\}$.*

Proof. Define the function $\chi(x, y, \theta) = -y$ so that it is defined in G^- and it is zero in Σ . Then $\mathcal{L}_{Z^-}\chi(p) = \xi(x, \theta) - \mu_d = 0$ on the line $\xi = \mu_d$, $\theta \in \mathbb{T}^1$. Moreover, $\mathcal{L}_{Z^-}^2\chi(p) = \cos\theta$. This is negative for $\theta \in]\pi/2, 3\pi/2[$ and positive for $\theta \in [0, \pi/2[$ and $\theta \in]3\pi/2, 2\pi[$. The points $\theta = \pi/2$ and $\theta = 3\pi/2$ have $\mathcal{L}_{Z^-}^2\chi(p) = 0$, but $\mathcal{L}_{Z^-}^3\sigma(p) \neq 0$. Similar computations prove the result for $Z^+(z)$. \square

Knowledge of the tangencies is sufficient to describe the local phase space of system (4) around the discontinuity Σ , as Figure 3 shows. Section 4 discusses how forward solutions of $Z(z)$, which are smooth within each set G^\pm and Σ_s , connect at the boundaries of these regions. It is futile to study solutions in backwards time because when an orbit lands on Σ_s , the information of when it landed is lost.

4. Forward Solutions of the Discontinuous System. Classical results on existence and uniqueness of solutions require Lipschitz continuous right-hand sides and therefore do not apply to discontinuous systems like (4). A class of discontinuous systems for which some results are known is that of Filippov type [19, (a) in section 4]. A Filippov-type system is a system where the linear convex combination of the vector fields $Z^\pm(z)$ is sufficient to describe the dynamics within the switching manifold Σ . Filippov's convex method is useful, especially when there is no vector field already defined on Σ .

Let $Z_y^\pm(z)$ be the y -component of $Z^\pm(z)$ at a point $z \in \Sigma$. Then Filippov's convex method defines the *crossing region* as the subset of Σ where $Z_y^+ \cdot Z_y^-(z) > 0$, while the *sliding region* $\Sigma_{s, \text{Filippov}}$ satisfies $Z_y^+ \cdot Z_y^-(z) < 0$ [19, section 4], [12, p. 76]. The idea

is that solutions inside the sliding region cannot exit Σ because $Z^\pm(z)$ do not allow it.

Remark 4.1. System (4) together with the friction law (5) is not of Filippov type. Indeed, the sliding region of system (4) is

$$\Sigma_{s,\text{Filippov}} := \{(x, y, \theta) \in \mathbb{R}^2 \times \mathbb{T}^1 \mid y = 0 \text{ and } -\mu_d < \xi < \mu_d\},$$

which is a strip within Σ_s whenever $\mu_d < \mu_s$. In the two remaining bands

$$\begin{aligned}\Sigma_{s,\text{stiction}}^- &:= \{(x, y, \theta) \in \mathbb{R}^2 \times \mathbb{T}^1 \mid y = 0 \text{ and } \xi \in]\mu_d, \mu_s[\}, \\ \Sigma_{s,\text{stiction}}^+ &:= \{(x, y, \theta) \in \mathbb{R}^2 \times \mathbb{T}^1 \mid y = 0 \text{ and } \xi \in]-\mu_s, -\mu_d[\},\end{aligned}$$

which are colored in gray in Figure 3(a), the vector field $Z_s(z)$ does not belong to the convex closure of $Z^\pm(z)$. Here Filippov's method predicts orbits that switch from G^+ to G^- or vice versa, but the actual solution of model (4) lies within Σ_s .

When $\mu_d = \mu_s$, the friction law (5) equals the classical Coulomb friction and Σ_s coincides with $\Sigma_{s,\text{Filippov}}$. This case has been studied in [10, 21, 33].

The two gray bands $\Sigma_{s,\text{stiction}}^\pm$ are unstable to perturbations in y in the following sense: consider, for instance, a point in $\Sigma_{s,\text{stiction}}^-$ that is *pushed* into G^- by an arbitrary small perturbation; this solution will evolve far from $\Sigma_{s,\text{stiction}}^-$ by following $Z^-(z)$. In this sense, the piecewise-smooth flow is not continuous with respect to the initial conditions.

Another notion of a forward solution of a discontinuous system is the *Carathéodory solution* [8], [19, section 1]. This is an absolutely continuous function $z(t)$ that satisfies

$$(7) \quad z(t) = z(0) + \int_0^t Z(z(s)) ds, \quad t \geq 0,$$

where the integral is in a Lebesgue sense. Hence, in order to have a Carathéodory solution, $Z(z)$ need only be defined almost everywhere.

PROPOSITION 4.2. *For every $z_0 = z(0) \in \mathbb{R}^2 \times \mathbb{T}^1$ there exists a global forward Carathéodory solution of model (4) satisfying (7) for every $t \geq 0$.*

Proof. For every z_0 there exists at least one local classical solution of either $Z^\pm(z)$ or $Z_s(z)$. A forward solution of (7) is obtained by piecing together such local orbits on Σ . This process produces a global solution since (a) $Z^\pm(z)$ and $Z_s(z)$ are each linear in (x, y) , excluding the possibility of blowup in finite time, and (b) there can be no accumulation points where the time intervals between switching converge to zero. \square

Not every forward Carathéodory solution has a physical meaning. Consider, for instance, a trajectory that under the forward flow (4) lands inside $\Sigma_{s,\text{stiction}}^-$, as shown in Figure 4(a). There are two ways to obtain a forward solution at this point: either leave Σ and follow the vector field $Z^-(z)$, or remain on Σ_s . In addition, the forward trajectory on Σ_s may switch to G^- at any point within $\Sigma_{s,\text{stiction}}^-$. The orbits switching to G^- appear to be mathematical artifacts, as they do not satisfy the condition $|\xi| > \mu_s$ of the stiction law (5). There is a need for a concept of solution that discards all these pathologies. The following definition does so by using a “minimal” approach.

DEFINITION 4.3. *A stiction solution $t \mapsto z(t)$, with $t \geq 0$, is a Carathéodory solution that leaves Σ_s only at the boundaries $\partial\Sigma_c^\pm$.*

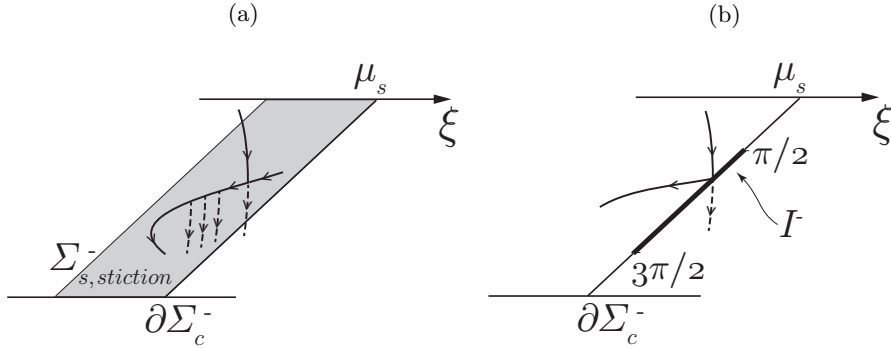


Fig. 4 (a) A Carathéodory solution with a pathological nondeterminacy of the forward motion on the gray band. (b) Stiction solutions interacting with the line of forward nonuniqueness I^- .

A stiction solution is called singular if, for some $t_1 \geq 0$, the point $z(t_1)$ belongs to one of the following sets:

$$\begin{aligned} I^+ &:= \{(x, y, \theta) \in \mathbb{R}^2 \times \mathbb{T}^1 \mid \xi = -\mu_s, y = 0, \theta \in [\pi/2, 3\pi/2[\}, \\ I^- &:= \{(x, y, \theta) \in \mathbb{R}^2 \times \mathbb{T}^1 \mid \xi = \mu_s, \quad y = 0, \theta \in [0, \pi/2[\cup [3\pi/2, 2\pi[\}. \end{aligned}$$

Otherwise, the stiction solution is called regular.

The sets I^\pm belong to the boundary lines $\partial\Sigma_c^\pm$. Three vector fields are defined on $\partial\Sigma_c^\pm$: $Z_s(z)$ and $Z^\pm(z)$. In particular, on both I^\pm the vector field $Z_s(z)$ points inside Σ_s , as follows from Proposition 3.2; compare with Figure 3(b). Proposition 4.4 describes the existence and uniqueness of stiction solutions for model (4).

PROPOSITION 4.4. *There exists a stiction solution $z(t)$ of problem (4) for any initial condition $z_0 = z(0) \in \mathbb{R}^2 \times \mathbb{T}^1$. Regular stiction solutions are forward unique, while singular stiction solutions are forward nonunique.*

Proof. It is clear that stiction solutions, as Carathéodory solutions, exist. Consider a trajectory $z(t)$ that reaches I^- at a time t_1 , as shown in Figure 4(b). Two different forward solutions satisfy (7): either leave Σ and follow the vector field $Z^-(z)$, or remain on Σ_s . Hence, the singular stiction solution is forward nonunique at I^- , and similarly at I^+ . On the contrary, if $z(t) \notin I^\pm$ at any $t \geq 0$, then there is always only one way to piece together the vector fields at the boundaries $\partial\Sigma_c^\pm$, and therefore $z(t)$ is forward unique. \square

The nonuniqueness of models with stiction friction was mentioned in [5, 50], without any further explanation. It is not possible to predict whether, for singular stiction solutions, the mass will slip or stick in forward time. Hence, numerical simulations that use stiction friction have to make a choice at the points of nonuniqueness to compute the forward flow, often without noticing that a choice is being made. This means that solutions may unknowingly be discarded. Section 5 investigates nonuniqueness by regularization.

5. Regularization. We consider the regularization of the vector field $Z(z)$ given by the one-parameter family $Z_\varepsilon(z)$ of smooth vector fields

$$(8) \quad Z_\varepsilon(z) := \frac{1}{2}Z^+(z)(1 + \phi(\varepsilon^{-1}y)) + \frac{1}{2}Z^-(z)(1 - \phi(\varepsilon^{-1}y))$$

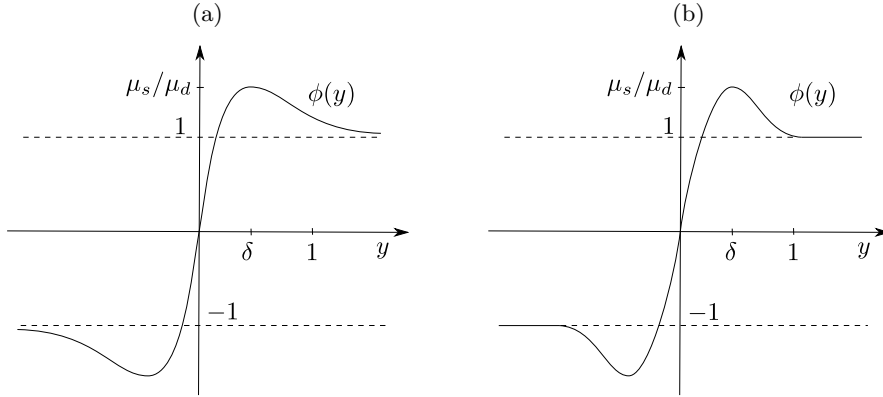


Fig. 5 (a) Regularization function satisfying (9) where $\phi(y) \rightarrow \pm 1$ as $y \rightarrow \pm\infty$. (b) Regularization function of Sotomayor–Teixeira type where ϕ reaches ± 1 at finite values $y = \pm 1$; see (20).

for $0 < \varepsilon \ll 1$. The function $\phi(y)$ is a sufficiently smooth *regularization function* that, based upon the physics of the problem, we will assume is odd and satisfies

$$(9) \quad \phi(y) \begin{cases} \rightarrow 1, & y \rightarrow \infty, \\ = \mu_s/\mu_d, & y = \delta, \end{cases} \quad \text{and} \quad \phi'(y) \begin{cases} > 0, & 0 < y < \delta, \\ = 0, & y = \delta, \\ < 0, & \delta < y < \infty, \end{cases} \quad \phi''(\delta) < 0,$$

for all $y \geq 0$, and where $\delta \in (0, 1)$.¹ Consequently, $y = \pm\delta$ is a global maximum/minimum of ϕ with values $\pm\mu_s/\mu_d \gtrless \pm 1$, respectively, and $\phi(y) \rightarrow \pm 1$ as $y \rightarrow \pm\infty$. See Figure 5(a) for an illustration. The regularized problem $z' = Z_\varepsilon(z)$ is smooth and consequently (locally) well-posed, and at the same time we will see that it “approximates” the discontinuous problem (4) for $0 < \varepsilon \ll 1$.

In noncompact form, $z' = Z_\varepsilon(z)$ is the singularly perturbed problem

$$(10) \quad \begin{aligned} x' &= y, \\ y' &= -\xi(x, \theta) - \mu_d \phi(\varepsilon^{-1}y), \\ \theta' &= 1, \end{aligned}$$

with $\xi(x, \theta) = \gamma^2 x + \sin \theta$ being the function introduced in section 2. By the first property of (9), it follows that

$$(11) \quad \lim_{\varepsilon \rightarrow 0} Z_\varepsilon(z) = Z^\pm(z) \quad \text{for } y \gtrless 0,$$

pointwise, so that the two problems coincide outside $y \neq 0$ in the limit $\varepsilon \rightarrow \infty$. On the other hand, when solutions of (10) enter the region of regularization, i.e., when $y = \mathcal{O}(\varepsilon)$, we can follow them in the rescaled coordinate \hat{y} defined by

$$(12) \quad y = \varepsilon \hat{y},$$

¹Notice that once we suppose $\delta > 0$ we can without loss of generality, upon scaling ε , take $\delta \in (0, 1)$.

so that $y = \mathcal{O}(\varepsilon)$ becomes $\hat{y} = \mathcal{O}(1)$. In this new scaling, system (10) becomes the multiple time scale problem

$$(13) \quad \begin{aligned} x' &= \varepsilon \hat{y}, \\ \varepsilon \hat{y}' &= -\xi(x, \theta) - \mu_d \phi(\hat{y}), \\ \theta' &= 1, \end{aligned}$$

which is also known as the *slow problem* [31, 43]. By introducing the fast time $\tau := t/\varepsilon$, system (13) is equivalent to the *fast problem*

$$(14) \quad \begin{aligned} \dot{x} &= \varepsilon^2 \hat{y}, \\ \dot{\hat{y}} &= -\xi(x, \theta) - \mu_d \phi(\hat{y}), \\ \dot{\theta} &= \varepsilon, \end{aligned}$$

with the overdot meaning differentiation with respect to the fast time τ . The standard procedure for solving multiple time scale problems is to combine the solutions of the *layer problem*

$$(15) \quad \dot{\hat{y}} = -\xi(x, \theta) - \mu_d \phi(\hat{y}), \quad (x, \theta)(\tau_0) = (x_0, \theta_0),$$

with those of the *reduced problem*

$$(16) \quad \begin{aligned} x' &= 0, \\ 0 &= -\xi(x, \theta) - \mu_d \phi(\hat{y}), \\ \theta' &= 1, \end{aligned}$$

where (15) and (16) are the limit for $\varepsilon \rightarrow 0$ of the fast and slow problems (14) and (13). The set of fixed points of the layer problem (15) is called the *critical manifold*,

$$(17) \quad C_0 := \{(x, \hat{y}, \theta) \in \mathbb{R}^2 \times \mathbb{T}^1 \mid \xi(x, \theta) + \mu_d \phi(\hat{y}) = 0\},$$

and the solutions of the reduced problem (16) are constrained to it. The critical manifold is said to be *normally hyperbolic* at the points where

$$\left. \frac{\partial \dot{\hat{y}}}{\partial \hat{y}} \right|_{C_0} = -\mu_d \phi'(\hat{y}^{C_0})$$

is nonzero and $\hat{y}^{C_0} = \phi^{-1}(-\xi(x, \theta)/\mu_d)$. It follows that C_0 is not normally hyperbolic on the two *fold lines*

$$f^\pm := \{(x, \hat{y}, \theta) \in \mathbb{R}^2 \times \mathbb{T}^1 \mid \xi = \mp \mu_s, \hat{y} = \pm \delta\}.$$

These lines separate C_0 into three normally hyperbolic subsets,

$$\begin{aligned} C_r^+ &:= \{(x, \hat{y}, \theta) \in C_0 \mid \delta < \hat{y} < \infty\}, \\ C_a &:= \{(x, \hat{y}, \theta) \in C_0 \mid -\delta < \hat{y} < \delta\}, \\ C_r^- &:= \{(x, \hat{y}, \theta) \in C_0 \mid -\infty < \hat{y} < -\delta\}, \end{aligned}$$

as shown in Figure 6, where C_a is attracting and C_r^\pm are repelling. Notice that C_a is a graph $\hat{y} \in]-\delta, \delta[$ over Σ_s , while C_r^+ (C_r^-) is a graph $\hat{y} > \delta$ ($\hat{y} < -\delta$) over $\Sigma_{s,\text{stiction}}^+$ ($\Sigma_{s,\text{stiction}}^-$, respectively). In terms of (x, y, θ) , these sets collapse onto Σ_s and $\Sigma_{s,\text{stiction}}^\pm$, respectively, as $\varepsilon \rightarrow 0$, since $y = \varepsilon \hat{y}$. Similarly, f^\pm collapse onto $\partial \Sigma_c^\pm$. This means that in the (x, y, θ) -space it is not possible to distinguish whether a trajectory belongs to C_a or to C_r^\pm for $\varepsilon = 0$.

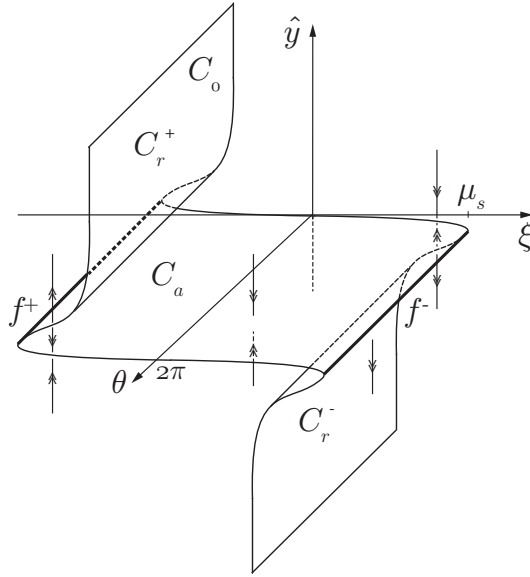


Fig. 6 Critical manifold C_0 and its stability properties. In bold: f^\pm . The double arrow denotes dynamics in the fast time τ .

PROPOSITION 5.1. *The reduced problem on C_0 coincides with the vector field $Z_s(z)$ on Σ_s .*

The proof is straightforward since the reduced problem, once constrained to C_0 , is $(x', \theta') = (0, 1)$.

The results of Fenichel [17, 18] guarantee that a normally hyperbolic, compact, and invariant manifold $S_0 \subset C_0$ perturbs into a nonunique and locally invariant *slow manifold* S_ε that is ε -close to S_0 for ε sufficiently small. Furthermore, system (14) has an invariant foliation with base on S_ε that is a perturbation of the foliation of the layer problem (15) with base on S_0 .

Consequently, it follows that the regularized problem (10) captures all the main features of the discontinuous vector field (4) for $\varepsilon \rightarrow 0$. Furthermore, when $0 < \varepsilon \ll 1$ the solutions of (10) are uniquely defined, so that the issue of nonuniqueness of (4) is eliminated. Proposition 5.1 also motivates the conditions (9) for the function $\phi(y)$ (see also Remark 5.2).

Nevertheless, formally the previous results in the scaling regime defined by (12) only cover $y = \mathcal{O}(\varepsilon)$, and, as can also be seen from the layer problem (15), this regime does not overlap with the regular perturbations of Z^\pm for $y = \mathcal{O}(1)$ as $\varepsilon \rightarrow 0$. In particular, following (11), Z^\pm sits at $\hat{y} = \pm\infty$ as $\varepsilon \rightarrow 0$. One way, based upon an adaptation of the blowup method, to cover Z_ε as $\varepsilon \rightarrow 0$ uniformly in y is described in the references [34, 36, 38, 40]. Summarizing, one considers the extended fast-time system

$$(18) \quad \begin{aligned} z' &= \varepsilon Z_\varepsilon, \\ \varepsilon' &= 0, \end{aligned}$$

which has a loss of smoothness along the switching manifold $\Sigma \times \{0\}$ in the extended

(z, ε) -space. We then apply a cylindrical blowup transformation of $\Sigma \times \{0\}$,

$$(19) \quad r \geq 0, (\bar{y}, \bar{\varepsilon}) \in S^1 \mapsto \begin{cases} y = r\bar{y}, \\ \varepsilon = r\bar{\varepsilon}, \end{cases}$$

where $S^1 : \bar{y}^2 + \bar{\varepsilon}^2 = 1$. In the blowup space, the system regains smoothness and the discontinuity set $\Sigma \times \{0\}$ is replaced by $\mathbb{R} \times \mathbb{T} \times S^1$. However, unlike in the classical blowup method, we perform (due to the special form of (18)) the *desingularization* of the blown up vector field by dividing the right-hand side by the common factor $\bar{\varepsilon}$ (rather than by a power of r). In this way, one then gains (partial) hyperbolicity along $r = \bar{\varepsilon} = 0$, which enables a general matching procedure between the two regimes using local hyperbolic methods.

Geometrically, the coordinates (\hat{y}, ε) defined by (12) can be viewed as a directional chart associated with the blowup (19) obtained by setting $\bar{\varepsilon} = 1$ such that

$$\bar{\varepsilon}^{-1} \bar{y} = \hat{y}.$$

In particular, \hat{y} for $\varepsilon = 0$ describe points on $(\bar{y}, \bar{\varepsilon}) \in S^1$ with $\bar{\varepsilon} > 0$, whereas $\hat{y} \rightarrow \pm\infty$ corresponds to $(\bar{y}, \bar{\varepsilon}) = (\pm 1, 0)$. These points are better described in the $\bar{y} = \pm 1$ charts, where the matching between $y = \mathcal{O}(1)$ and $y = \mathcal{O}(\varepsilon)$ is performed.

For further details, we refer the reader to [36, 38, 40]. Here we will instead follow an adaptation of the regularization approach of Sotomayor–Teixeira (ST) [45, 60] (see also Remark 5.2) and henceforth we make the following additional, simplifying assumption: the function ϕ (9) is not asymptotic to ± 1 as $y \rightarrow \infty$ but instead reaches the following values at $y = \pm 1$:

$$(20) \quad \phi(y) = \pm 1 \quad \text{for all } y \gtrless \pm 1.$$

Furthermore, we suppose that $\phi^{(k)}(\pm 1) = 0$ for all $k = 1, \dots, n$, with n being sufficiently large for the forthcoming theory of smooth systems to apply. See Figure 5(b) for an illustration of a regularization function satisfying (20).

Following the work of [34, 36, 38, 40], the results remain qualitatively unchanged by the somewhat unnatural (from an application point of view) assumption (20). Technically, however, the problem is made significantly easier by (20) since we do not have to work with the full blowup transformation and the charts $\bar{\varepsilon} = \pm 1$. Specifically, by (20) we have that $Z_\varepsilon(z) = Z^\pm(z)$ for all $y \gtrless \pm\varepsilon$ and in the coordinates (\hat{y}, ε) the regularized system is therefore (naturally) compactified to $\hat{y} \in [-1, 1]$. For simplicity, we will therefore focus in what follows on regularization functions that satisfy (20).

Remark 5.2. The classical ST regularization considers a regularization function $\phi^{ST}(y)$ with $\phi^{ST}(y) = \pm 1$ for $y \gtrless \pm 1$ that is monotonously increasing within $y \in]-1, 1[$ [60]. Applying this regularization to our model (4) gives, in the singular limit $\varepsilon \rightarrow 0$, that the regularization $Z_\varepsilon^{ST}(z)$ has an attracting invariant manifold C_a^{ST} that is a graph of \hat{y} over $\Sigma_{s,\text{Filippov}}$ [35, 45]. In terms of (x, y, θ) this set collapses onto $\Sigma_{s,\text{Filippov}}$ instead of Σ_s , and hence $Z_\varepsilon^{ST}(z)$ does not tend to $Z(z)$ as $\varepsilon \rightarrow 0$. For this reason the classical ST regularization is inadequate for model (4).

Let $\varphi_t(z_0)$ be a regular stiction solution of model (4) with an initial condition in z_0 , and let $\varphi_t^\varepsilon(z_0)$ be the solution of the regularized problem (10) for the same initial condition. The following statement relates these two solutions.

PROPOSITION 5.3. *Consider system (10) with ϕ satisfying (9) as well as (20). Then for any $T > 0$ there exists an $\varepsilon_0 > 0$ such that the distance between the two solutions $\varphi_t^\varepsilon(z_0)$ and $\varphi_t(z_0)$ is bounded by $|\varphi_t^\varepsilon(z_0) - \varphi_t(z_0)| \leq c(T)\varepsilon^{2/3}$ for $t \in [0, T]$, $0 < \varepsilon \leq \varepsilon_0$. Here $c(T)$ is a constant that depends upon T .*

Proof. Fenichel's theorems guarantee that, sufficiently far from the fold lines f^\pm , the orbit $\varphi_t^\varepsilon(z_0)$ of the slow-fast problem (13) is $O(\varepsilon)$ -close to the singular trajectory $\varphi_t(z_0)$. At the folds f^\pm , if at the singular level the solutions are unique, the result by Szmolyan and Wechselberger [62, Theorem 1] guarantees that the distance between the two trajectories is bounded by $O(\varepsilon^{2/3})$ for a finite time interval T . This is the case of regular stiction solutions. \square

The following proposition relates the family of sticking solutions of Corollary 3.3 with a family of trajectories on the slow manifold for the regularized problem. For this, define $S_a \subset C_a$ as the compact, normally hyperbolic set $S_a := \{(x, \hat{y}, \theta) \in \mathbb{R}^2 \times \mathbb{T}^1 \mid |\gamma^2 x| \leq \mu_s - 1 - c, \xi(x, \theta) + \mu_d \phi(\hat{y}) = 0\}$ for $\mu_s > 1$ with $c \in \mathbb{R}^+$ fixed so small that S_a is nonempty. The set S_a is a graph over the set of invariant circles of Corollary 3.3 for $c \rightarrow 0$.

PROPOSITION 5.4. *Suppose (9) and, specifically, that ϕ is odd. Then the compact critical manifold S_a perturbs into a slow manifold $S_{a,\varepsilon}$ for all $0 < \varepsilon \ll 1$ and on it there exists a unique, attracting 2π -periodic limit cycle passing through $(x, \theta) = (O(\varepsilon), 0)$.*

Proof. From Proposition 5.1 and Corollary 3.3 it follows that S_a is filled by circular trajectories. By Fenichel's results, when $0 < \varepsilon \ll 1$ the submanifold S_a perturbs into the graph $\hat{y} = \phi^{-1}(-\xi(x, \theta)/\mu_d) + \varepsilon h_1(x, \theta, \varepsilon)$ with h_1 smooth. On this graph the slow problem (13) is a 2π -periodic, nonautonomous ODE for $x(\theta)$, where θ has the meaning of time:

$$(21) \quad x'(\theta) = \varepsilon \phi^{-1} \left(\frac{-\xi(x, \theta)}{\mu_d} \right) + \varepsilon^2 h_1(x, \theta, \varepsilon).$$

Fix a global Poincaré section at $\theta = 0$ and define the return map $P(x(0), \varepsilon) = x(2\pi)$. The fixed points of this map for $0 < \varepsilon \ll 1$ are the zeros of the Melnikov-like function

$$Q(x(0), \varepsilon) := \frac{P(x(0), \varepsilon) - x(0)}{\varepsilon} = \int_0^{2\pi} \phi^{-1} \left(\frac{-\gamma^2 x(s) - \sin s}{\mu_d} \right) ds + O(\varepsilon),$$

where the last equality is obtained by integrating (21). For $\varepsilon = 0$, (21) implies $x(\theta) = x(0)$ for all $\theta \in \mathbb{T}^1$. By assumption, both functions $\phi^{-1}(s)$ and $\sin s$ are odd functions of s . This means that $Q(x(0), 0) = 0$ if and only if $x(0) = 0$. Furthermore, $(x, \varepsilon) = (0, 0)$ is regular because

$$(22) \quad \partial_x Q(0, 0) = -\frac{\gamma^2}{\mu_d} \int_0^{2\pi} \frac{1}{\phi'(-\sin s/\mu_d)} ds < 0$$

and $\phi'(\hat{y})$ is always positive in S_a since $\hat{y} \in]-\delta, \delta[$. Then the implicit function theorem guarantees that for $0 < \varepsilon \ll 1$ there exists $x(0) = m(\varepsilon)$ such that $Q(m(\varepsilon), \varepsilon) = 0$. Hence, $x(0) = m(\varepsilon)$ belongs to an attracting periodic orbit since from (22) it follows that $|\partial_{x(0)} P(x(0), \varepsilon)| < 1$ for $0 < \varepsilon \ll 1$. \square

Therefore, when $\mu_s > 1$ the family of invariant circles in Σ_s bifurcates into a single attracting limit cycle on the slow manifold $S_{a,\varepsilon}$. This result gives an upper bound of the time T of Proposition 5.3 as a function of ε , since on the slow manifold

$S_{a,\varepsilon}$, after a time $t = O(1/\varepsilon)$, orbits are $O(1)$ distant to the original family of circles in Σ_s . Furthermore, the regularization of regular stiction solutions does not necessarily remain uniformly close.

It is not possible to make a statement similar to Proposition 5.3 for singular stiction solutions, as they have nonunique forward solutions at the singular level. A further understanding can be obtained by studying the reduced problem (16). This differential algebraic equation is rewritten as a standard ODE by explicating the algebraic condition with respect to x and by differentiating it with respect to the time t :

$$(23) \quad \begin{aligned} -\mu_d \phi'(\hat{y}) \hat{y}' &= \cos \theta, \\ \theta' &= 1. \end{aligned}$$

PROPOSITION 5.5. *The circles $f^\pm \subset \{\phi'(\hat{y}) = 0\}$ are lines of singularities for the reduced problem (23), and solutions reach them in finite time. On f^\pm , the points $(\hat{y}, \theta) = (-\delta, \pi/2)$ and $(\hat{y}, \theta) = (\delta, 3\pi/2)$ are folded saddles, while $(\hat{y}, \theta) = (\delta, \pi/2)$ and $(\hat{y}, \theta) = (-\delta, 3\pi/2)$ are folded centers. Moreover, the intervals $\hat{I}^\pm \subset f^\pm$ defined as*

$$\begin{aligned} \hat{I}^- &:= \{(x, \hat{y}, \theta) \in \mathbb{R}^2 \times \mathbb{T}^1 \mid \xi = \mu_s, \quad \hat{y} = -\delta, \theta \in [\pi/2, 3\pi/2[\}, \\ \hat{I}^+ &:= \{(x, \hat{y}, \theta) \in \mathbb{R}^2 \times \mathbb{T}^1 \mid \xi = -\mu_s, \quad \hat{y} = \delta, \quad \theta \in [0, \pi/2[\cup [3\pi/2, 2\pi[\} \end{aligned}$$

have nonunique forward solutions.

Proof. The time transformation $\mu_d \phi'(\hat{y}) d\hat{t} = dt$ allows one to rewrite system (23) as the *desingularized problem*

$$(24) \quad \begin{aligned} \dot{\hat{y}} &= -\cos \theta, \\ \dot{\theta} &= \mu_d \phi'(\hat{y}) \end{aligned}$$

in the new time \hat{t} . The difference between systems (23) and (24) is that \hat{t} reverses the direction of time within C_r^\pm . Problem (24) has four fixed points in $\mathbb{R}^2 \times \mathbb{T}^1$. The points $(\delta, 3\pi/2)$ and $(-\delta, \pi/2)$ are hyperbolic saddles with eigenvalues $\pm\sqrt{\mu_d|\phi''(\delta)|}$ and eigenvectors $[1, \mp\sqrt{\mu_d|\phi''(\delta)|}]^T$ and $[1, \pm\sqrt{\mu_d|\phi''(\delta)|}]^T$, respectively. The remaining points $(\delta, \pi/2)$ and $(-\delta, 3\pi/2)$ are centers with eigenvalues $\pm i\sqrt{\mu_d|\phi''(\delta)|}$ and eigenvectors $[1, \pm i\sqrt{\mu_d|\phi''(\delta)|}]^T$ and $[1, \mp i\sqrt{\mu_d|\phi''(\delta)|}]^T$, respectively. The inversion of the time direction on C_r^\pm gives the dynamics of the reduced problem (23). Thus, a saddle in (24) is a folded saddle of (23), and similarly for the centers. Also, f^\pm become lines of singularities with the time inversion, and the segments \hat{I}^\pm have forward trajectories pointing inside both C_a and C_r^\pm ; compare with Figure 7(a). Since $\theta' = 1$, orbits reach or leave f^\pm in finite time. \square

Figure 7 illustrates the results of Proposition 5.5. In the (x, y, θ) coordinates, the segments \hat{I}^\pm collapse onto the lines of nonuniqueness I^\pm for $\varepsilon = 0$. The layer problem (15) adds a further forward solution in \hat{I}^\pm since orbits may also leave a point of these lines by following a fast fiber for $\hat{y} \gtrless 0$.

Each folded saddle of (23) has two special solutions: the *singular vrai canard* Υ^v , a stable manifold of (24) that connects C_a to C_r^\pm , and the *singular faux canard* Υ^f , an unstable manifold of (24) that does the opposite [3, 15]. The vrai canard divides the critical manifold into regions with different types of forward dynamics: on one side of Υ^v , orbits *turn*, which means that they remain on C_a . On the other

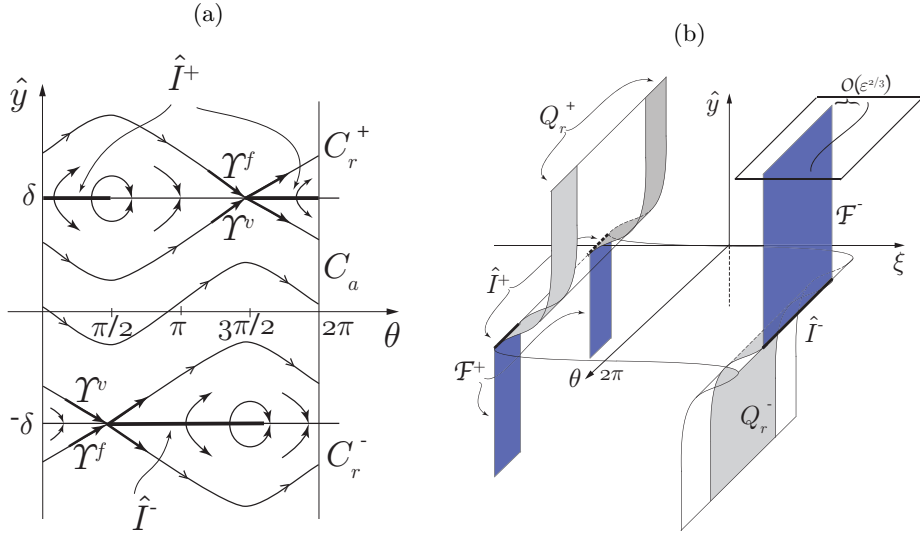


Fig. 7 (a) Phase space of the reduced problem (23). (b) Repelling invariant manifolds Q_r^\pm in gray and foliations F^\pm in blue.

side of γ^v , orbits reach $f^\pm \setminus \hat{I}^\pm$ and then *jump*; that is, they move away from C_0 by following a fast fiber. Taken together the singular canards form a periodic orbit of the reduced problem (23) that visits both C_a and C_r^\pm ; see Figure 7(a). The folded centers have no canard solutions [42], and for this reason they are not interesting for the analysis. Systems with $m \geq 2$ slow variables and one fast variable have robust canard solutions; i.e., the canards persist for small parameter variations. It follows that canard solutions are a generic feature of (12), where $m = 2$, appearing for any regularization function (9). Canards also appear in the Van der Pol oscillator [22, 65], in a model for global warming [66], and in a model for transonic wind [7].

In our case, we consider system (9) with any ϕ satisfying (10) and suppose $0 < \varepsilon \ll 1$. Then the singular vrai canard γ^v perturbs into a maximal canard [61]. This orbit corresponds to the intersection of $S_{a,\varepsilon}$ with $S_{r,\varepsilon}^\pm$. Hence, the maximal canard remains $O(\varepsilon)$ -close to S_r^\pm for a time $t = O(1)$. Furthermore, a family of orbits remains exponentially close to the maximal canard for some time before being repelled from $S_{r,\varepsilon}^\pm$ [43, p. 200]. An orbit of this family is called a *canard*, and Figure 8(a) shows an example of one. Define Q_r^\pm as the subsets of C_r^\pm whose points, when flowed backwards in time, intersect the intervals of nonuniqueness \hat{I}^\pm . Q_r^\pm are colored in gray in Figure 7(b). The lines \hat{I}^\pm are, backwards in time, the base of a foliation of fast (nonhyperbolic) fibers F^\pm that are colored in blue in Figure 7(b). The following proposition describes the role of the repelling manifolds Q_r^\pm for $0 < \varepsilon \ll 1$.

PROPOSITION 5.6. *For $0 < \varepsilon \ll 1$, compact subsets S_r^\pm of Q_r^\pm perturb into the sets $S_{r,\varepsilon}^\pm$ that are $O(\varepsilon)$ -close to S_r^\pm . The slow problem on $S_{r,\varepsilon}^\pm$ is connected backwards in time to a family of fast trajectories F_ε^\pm that is $O(\varepsilon^{2/3})$ -close to F^\pm . The orbits on F_ε^\pm and $S_{r,\varepsilon}^\pm$ separate the trajectories that, after possibly having been exponentially close to $S_{r,\varepsilon}^\pm$, are attracted to the slow manifold $S_{a,\varepsilon}$ from the trajectories that follow a fast trajectory away from the slow surface.*

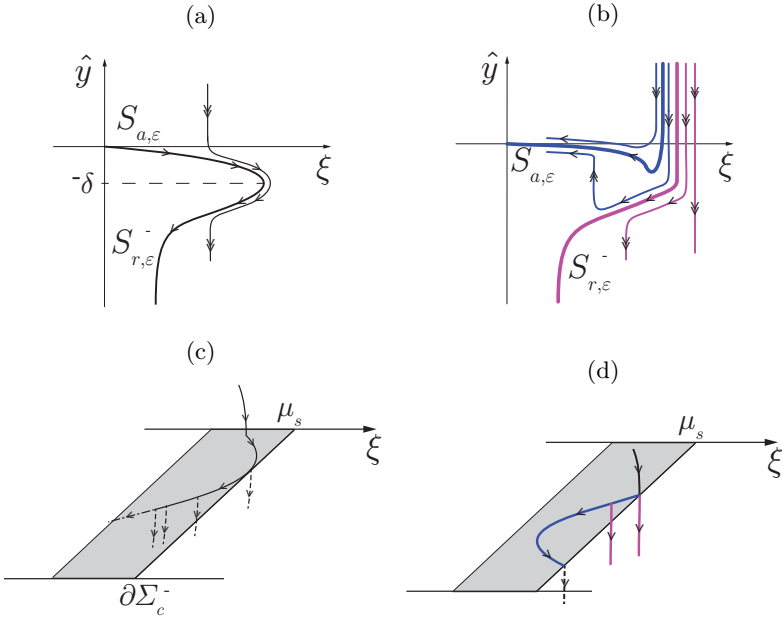


Fig. 8 (a) A canard orbit at the intersection of $S_{a,\varepsilon}$ with $S_{r,\varepsilon}^-$. (b) Dynamics around a point of \hat{I}^- for $0 < \varepsilon \ll 1$. (c) and (d) The same dynamics of Figures 8(a) and 8(b) in the (x, y, θ) -coordinates. The canard-like solutions leaving $\Sigma_{s,stiction}^-$ resemble Carathéodory solutions of model (4); compare with Figure 4(a).

Proof. By reversing the time orientation on the slow (13) and fast (14) problems, the orbits on Q_r^\pm satisfy the assumptions of Proposition 5.3. Hence, the distance from $\mathcal{F}_\varepsilon^\pm$ to $\mathcal{F}_\varepsilon^\pm$ is $O(\varepsilon^{2/3})$. Now consider again the true time direction and take a set of initial conditions that is exponentially close to the fibers $\mathcal{F}_\varepsilon^\pm$. These orbits will follow the repelling slow manifolds $S_{r,\varepsilon}^\pm$ for a time $t = O(1)$ [61]. The manifolds $S_{r,\varepsilon}^\pm$ act as separators of two different futures: on one side the orbits will become attracted to the slow attracting manifold $S_{a,\varepsilon}$, while on the other side they will jump away by following an escaping fast fiber; compare with Figure 8(b). \square

It follows that around \hat{I}^\pm and \mathcal{F}^\pm there is a high sensitivity to the initial conditions. Even though the (x, θ) -dynamics on C_a coincides with that on C_r^\pm , trajectories close to these two manifolds may have different futures. Orbits belonging to $S_{a,\varepsilon}$ will exit $S_{a,\varepsilon}$ at a predictable point. On the other hand, the orbits that follow $S_{r,\varepsilon}^\pm$ are very sensitive and may escape from it at any time. These two types of trajectories are colored in blue and magenta, respectively, in Figures 8(b) and 8(d). The orbits that follow $S_{r,\varepsilon}^\pm$ for some time are canard-like in their forward behavior. However, in backwards time they are connected to a family of fast fibers instead of to $S_{a,\varepsilon}$, and for this reason they are not typical canards like Υ^v .

We complete this section by making the following important remarks on the connection to the piecewise-smooth system and the stiction solutions: In the original coordinates (x, y, θ) , the canard trajectories of the folded saddles and the canard-like solutions of the lines \hat{I}^\pm leave the slow manifold at a point inside $\Sigma_{s,stiction}^\pm$, as in Figures 8(c) and 8(d). In the $\varepsilon = 0$ limit, we can identify these trajectories as orbits $(x, \theta)(t)$ of Z_s within $\Sigma : y = 0$ that satisfy the Carathéodory condition

(7). However, they are *not* stiction solutions. It follows that some of the a priori nonphysical Carathéodory solutions of (4) appear upon regularization of the stiction model: these are the trajectories of Z_s that intersect I^\pm backwards in time. All the other Carathéodory solutions of model (4) do not have a corresponding solution in the regularized model. These statements are all independent of the regularization function ϕ .

The physical interpretation of the solutions with canard is that the slip onset is delayed with respect to the time when the external forces have equaled the maximum static friction force. Figure 11(c) in subsection 6.1 shows a numerical solution with this delay.

6. Slip-Stick Periodic Orbits. This section considers a family of periodic orbits of model (4) that interacts with the lines of nonuniqueness I^\pm . Then subsection 6.1 discusses how the family perturbs in the regularized system (10) for $0 < \varepsilon \ll 1$ by combining numerics and analysis.

Model (4) has several kinds of periodic motion: pure slip [9, 59], pure stick [26], nonsymmetric slip-stick [2, 20, 48, 49, 52], and symmetric slip-stick [26, 49]. This section focuses on the latter, as slip-stick orbits are likely to be affected by the nonuniqueness at I^\pm . Figure 9 shows an example of such a trajectory. The symmetric slip-stick trajectories can be found by solving a system of algebraic equations, because system (4), in its nonautonomous form, is piecewise-linear in each region. Furthermore, it is sufficient to study only half the period, as ensured by Lemmas 6.1 and 6.2.

LEMMA 6.1. *System (4) has a symmetry*

$$(25) \quad S(x, y, \theta) = (-x, -y, \theta + \pi).$$

Proof. The map (25) is a diffeomorphism $\mathbb{R}^2 \times \mathbb{T}^1 \rightarrow \mathbb{R}^2 \times \mathbb{T}^1$ that satisfies the condition for a symmetry $Z(S(z)) = DS(z)Z(z)$, where $DS(z)$ is the Jacobian of $S(z)$ and $z = (x, y, \theta)$ [46, p. 211]. \square

LEMMA 6.2. *Let $\varphi_t(z)$ be the regular stiction orbit of system (4) at time t with initial condition $z = (x, y, \theta)$. If $\varphi_\pi(z) = (-x, -y, \theta + \pi)$, then the orbit is symmetric and periodic with period $T = 2\pi$.*

Proof. Applying the symmetry map (25) to the point $\varphi_\pi(z)$ gives

$$S(-x, -y, \theta + \pi) = (x, y, \theta + 2\pi).$$

Since $Z(x, y, \theta + 2\pi) \equiv Z(x, y, \theta)$ for any $\theta \in \mathbb{T}^1$, the flow $\varphi_t(z)$ is symmetric and periodic, with symmetry (25) and period $T = 2\pi$. \square

The results of Lemma 6.2 have been used in [59] even though the symmetry is not made explicit. Define $\varphi_t^{\text{slip}}(z_0)$ (resp., $\varphi_t^{\text{stick}}(z_1)$) as the slip (stick) solution of $Z^-(z)$ ($Z_s(z)$) with initial conditions in z_0 (z_1). The following lemma states the conditions under which these two solutions, pieced together, belong to a symmetric slip-stick periodic orbit.

LEMMA 6.3. *Necessary conditions for the slip and stick solutions $\varphi_t^{\text{slip}}(z_0)$ and $\varphi_t^{\text{stick}}(z_1)$ to form the lower half of a symmetric, slip-stick, periodic orbit are*

$$(26a) \quad \varphi_{\pi-\theta^*}^{\text{slip}}(z_0) = \varphi_0^{\text{stick}}(z_1),$$

$$(26b) \quad \varphi_{\theta^*}^{\text{stick}}(z_1) = S(z_0),$$

where $0 < \theta^* < \pi$ is the duration of one stick phase and $z_0 \in \partial\Sigma_c^-$, $z_1 \in \Sigma_s$.

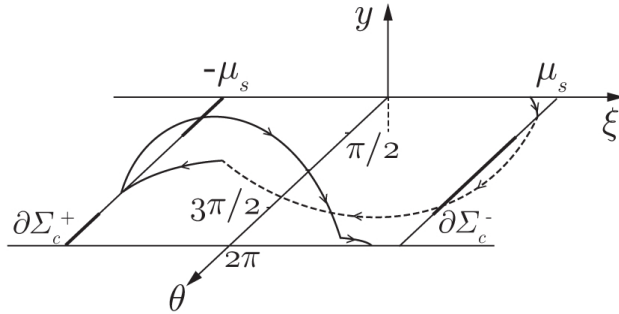


Fig. 9 A symmetric, slip-stick, periodic orbit with $\theta \in \mathbb{T}^1$. The dashed line represents trajectories in Z^- . The interest lies in studying how such an orbit interacts with the intervals of nonuniqueness I^\pm (in bold) under variation of a parameter.

Table I Parameter values used in the simulations.

System	μ_s	μ_d	ε	δ	a	b	c	d
Nonsmooth (4)	1.1	0.4						
Regularized (10)	1.1	0.4	10^{-3}	0.6	10.5766	-16.9937	1.7575	5.6595

Condition (26a) guarantees the continuity between the stick and slip phases, while (26b) guarantees the symmetry. The upper half-period of the orbit follows by applying the symmetry map (25) to φ_t^{slip} and φ_t^{stick} .

COROLLARY 6.4. *Conditions (26) are equivalent to*

$$(27a) \quad x^{\text{slip}}(\pi - \theta^*) = -x_0,$$

$$(27b) \quad y^{\text{slip}}(\pi - \theta^*) = 0,$$

$$(27c) \quad \pi - \theta^* + \theta_0 = \theta_1,$$

where $z_0 = (x_0, y_0, \theta_0) \in \Sigma_c^-$, $z_1 = (x_1, y_1, \theta_1) \in \Sigma_s$, and $\varphi_t^{\text{slip}}(z_0) = (x(t), y(t), \theta(t))^{\text{slip}}$.

Proof. The stick solution of (4) with initial condition $z_1 = (x_1, 0, \theta_1)$ is given by $(x, y, \theta)^{\text{stick}}(t) = (x_1, 0, t + \theta_1)$. Condition (26a) then implies that $x^{\text{slip}}(\pi - \theta^*) = x_1$ and $y^{\text{slip}}(\pi - \theta^*) = 0$, while $\theta^{\text{slip}}(\pi - \theta^*) = \pi - \theta^* + \theta_0 = \theta_1$. Condition (26b) adds, furthermore, that $x_1 = -x_0$. \square

The slip-stick solutions of (4) are now investigated numerically. The system of conditions (27) has five unknown parameters: $\gamma, \theta_0, \theta^*, \mu_s$, and μ_d . It is reasonable to fix μ_s and μ_d , since these are related to the material used, and then find a family of solutions of (27) by varying the frequency ratio $\gamma = \Omega/\omega$. The values used in the computations are listed in Table 1. Notice that conditions (27) are necessary but not sufficient: further admissibility conditions may be needed. These are conditions that ensure that each piece of solution does not exit its region of definition; for example, the stick solution should not cross $\partial\Sigma_c^-$ before $t = \theta^*$, and should not cross $\partial\Sigma_c^+$ for any $t \in [0, \theta^*]$. A numerical computation shows that system (27) has two branches of solutions $\Pi_0^{l,r}$, as shown in Figure 10: one for $\gamma < 1$ and one for $\gamma > 1$. The branches are disconnected around the resonance for $\gamma = 1$, where chaotic behavior

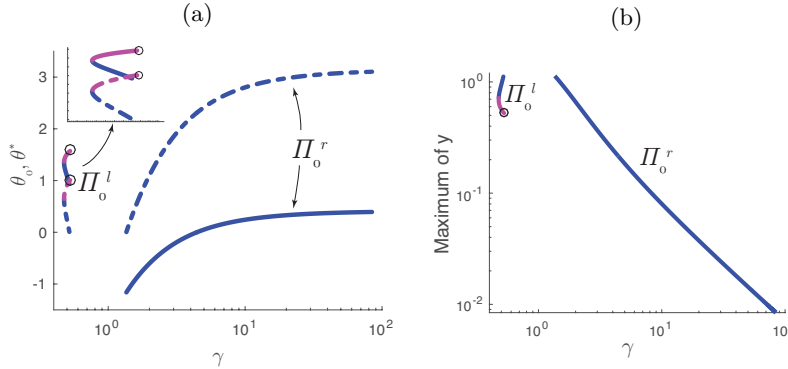


Fig. 10 (a) Two families of slip-stick orbits $\Pi_0^{l,r}$ of (4) for $\mu_s = 1.1$, $\mu_d = 0.4$. The solid line is θ_0 , while the dashed line is θ^* . The blue denotes a stable periodic orbit, while the magenta denotes a saddle periodic orbit. (b) Maximum amplitude of the orbits.

may appear [2, 9, 48]. The branch Π_0^l for $\gamma < 1$ is bounded by pure slip orbits when $\theta^* \rightarrow 0$ and by the visible tangency on Σ_s when $\theta_0 \rightarrow \pi/2$. The latter is marked with a circle in Figure 10(a). The branch Π_0^r for $\gamma > 1$ is delimited by pure slip orbits when $\gamma \rightarrow 1$, since again $\theta^* \rightarrow 0$, while when $\gamma \gg 1$, which is the rigid body limit, the family is bounded by $\theta^* \rightarrow \pi$. Here periodic orbits have a very short slip phase and an almost π -long stick phase.

A slip-stick orbit of model (4) has three Floquet multipliers: one is trivially unitary, the second one is always zero, and the last indicates the stability of the periodic orbit. The zero multiplier is due to the interaction of the periodic orbit with the sticking manifold Σ_s : solutions lying on this surface are backwards nonunique. Figure 10 denotes in blue the attracting periodic solutions and in magenta the repelling ones. In particular, the family Π_0^l becomes unstable sufficiently close to the visible tangency at $\theta_0 = \pi/2$, which is marked with a circle in Figure 10. This is because the visible tangency acts as a separatrix of two very different behaviors: on one side orbits jump, while on the other side they turn; recall Figure 7(a).

6.1. Slip-Stick Periodic Orbits in the Regularized System. This section finds slip-stick periodic solutions of the regularized model (10) with a numerical continuation in AUTO [11]. The solutions are then compared with those of the discontinuous system (4). The regularization function ϕ used is of the form (20), being a polynomial

$$\phi(y) = y(ay^6 + by^4 + cy^2 + d),$$

within $y \in [-1, 1]$. The coefficients a, b, c, d are therefore determined by the conditions in (9) and (20), and the specific values used in the simulations are listed in Table 1. The function ϕ is therefore C^∞ everywhere except at $y = \pm 1$. Here all one-sided derivatives exist, but only the first derivative is continuous there and, consequently, ϕ is therefore only C^1 . Figure 11(a) shows the family of slip-stick periodic orbits Π_ε of system (10). This can be seen, loosely, as the union of three branches,

$$\Pi_\varepsilon = \Pi_\varepsilon^l \cup \Pi_\varepsilon^c \cup \Pi_\varepsilon^r,$$

where $\Pi_\varepsilon^{l,r}$ are $O(\varepsilon^{2/3})$ -close to the regular branches $\Pi_0^{l,r}$ [62]. The branch Π_ε^c connects Π_ε^l to Π_ε^r at the rigid body limit, which is $\gamma \gg 1$, and it consists of slip-stick periodic

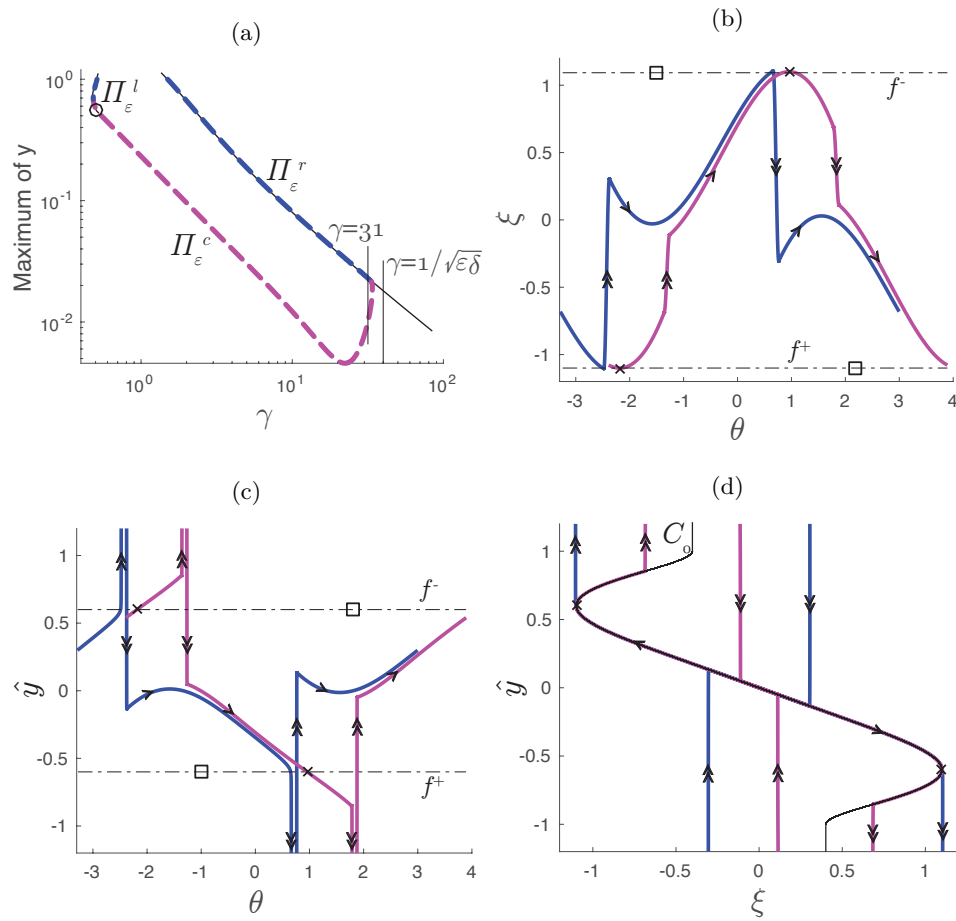


Fig. 11 Numerical simulation in AUTO. (a) Dashed line: the family Π_ε^l . The repelling branch Π_ε^c connects the two regular branches $\Pi_\varepsilon^{l,r}$. Solid line: families $\Pi_0^{l,r}$. The colors denote the stability of the orbits, as in Figure 10. (b) Two periodic orbits coexisting for $\gamma = 31$: a regular slip-stick in blue and a slip-stick with canard segments in magenta. The x marks the folded saddle, while the \square denotes the folded node. (c) and (d) Projections of (b) in the (θ, \hat{y}) - and (ξ, \hat{y}) -planes.

orbits each having two canard segments. Figures 11(b) to 11(d) show for $\gamma = 31$ two coexisting periodic orbits: the magenta one belongs to Π_ε^c , and the blue one belongs to Π_ε^r . In particular, Figure 11(c) shows the delay in the slip onset, when the orbit follows the canard, since the slip happens after a time $t = O(1)$ with respect to when the orbit has intersected the fold lines f^\pm .

Remark 6.5. Recall from (17) that trajectories on C_0 satisfy $\xi(x, \theta) = -\mu_d \phi(\hat{y})$. By Fenichel's results, a compact, normally hyperbolic submanifold $S_0 \subset C_0$ perturbs into a slow manifold S_ε for $0 < \varepsilon \ll 1$, and the flow on S_ε converges to the flow of (16) as $\varepsilon \rightarrow 0$. It follows that the time evolution of $\xi(x, \theta)$ is equivalent to evolution of the friction force up to $O(\varepsilon)$ terms; see Figures 11(b) and 11(d). In these figures, though, the vertical segments do not lie on S_ε , but are the projections of the fast fibers onto S_ε , and these are denoted with a double arrow.

The existence of the branch Π_ε^c is supported by Proposition 6.6 below. For this, let Σ_{out} be a cross-section orthogonal to the y -axis such that the fast fibers with base on the singular vrai canard on C_r^- intersect it on the line $L_{\text{out},0}$. Furthermore, define Σ_{in} as the cross-section orthogonal to the ξ -axis such that it intersects C_a on the line $L_{\text{in},0}$; see Figure 12(a).

PROPOSITION 6.6. *Suppose that there exists a smooth return mechanism $R : \Sigma_{\text{out}} \rightarrow \Sigma_{\text{in}}$ that maps $L_{\text{out},0} \subset \Sigma_{\text{out}}$ bijectively into $L_{\text{in},0} \subset \Sigma_{\text{in}}$ for $\varepsilon = 0$. Suppose, furthermore, that $L_{\text{in},0} = R(L_{\text{out},0})$ is transversal to the singular vrai canard Υ^v . Then for $0 < \varepsilon \ll 1$ there exists a locally unique orbit $\varphi_t^\varepsilon(z)$ that has a canard segment, and which tends to the singular canard for $\varepsilon \rightarrow 0$. Furthermore, this orbit has a saddle stability with Floquet multipliers: $\{1, O(e^{-c_1/\varepsilon}), O(e^{c_2/\varepsilon})\}$ with $c_{1,2} \in \mathbb{R}^+$.*

Proof. First notice that $R(\Sigma_{\text{out}})$ is an exponentially thin tubular neighborhood within Σ_{in} of a line segment $L_{\text{in},\varepsilon} = S_{a,\varepsilon} \cap \Sigma_{\text{in}}$. Notice also, by Fenichel's theory and the assumption of transversality, that $L_{\text{in},\varepsilon}$ is smoothly $O(\varepsilon)$ -close to $L_{\text{in},0}$ and contains the intersection of a maximal canard with Σ_{in} . This canard is the base of a smooth foliation of fibers, say $\mathcal{F}_{\Upsilon^v,\varepsilon}$, transverse to $L_{\text{in},\varepsilon}$. The foliation intersects Σ_{out} in a curve $L_{\text{out},\varepsilon}$ that is at least $C^1 O(\varepsilon^{2/3})$ -close to $L_{\text{out},0}$. Therefore, upon mapping $L_{\text{out},\varepsilon}$ forward using R , we obtain a unique transverse intersection of $R(L_{\text{out},\varepsilon})$ with $\mathcal{F}_{\Upsilon^v,\varepsilon}$ within Σ_{in} for each $0 \leq \varepsilon \ll 1$. Let q_ε denote the corresponding point on Σ_{out} . We then proceed as in the proof of canards in the planar setting; see [41]. In particular, by the blowup analysis in [61], it follows that there is small section Σ_{fold} at the folded saddle transverse to the fold line, described in the coordinates of the associated scaling chart, as well as a small neighborhood N_ε of q_ε such that the following holds: The backward and forward flows of N_ε intersect Σ_{fold} . The existence of a periodic orbit then becomes a root-finding problem. The existence of the root follows from an implicit function theorem argument. In particular, q_0 gives a root for $\varepsilon = 0$ which is nondegenerate. To explain the latter, we consider the variational equations and first take variations along $L_{\text{out},\varepsilon}$. This gives exponential decay in backward time but produces—by the transversality of $R(L_{\text{out},\varepsilon})$ with $L_{\text{in},\varepsilon}$ —a nonzero tangent vector to $S_{a,\varepsilon}$ at Σ_{fold} in forward time. Next, we take variations in a direction transverse to $L_{\text{out},0}$ at q_0 . At Σ_{fold} , this produces a nonzero tangent vector to $S_{r,\varepsilon}$ in backward time, and in combination this then gives the nondegeneracy of the root q_0 since these vectors, by the transversality of $S_{a,\varepsilon}$ and $S_{r,\varepsilon}$ along the vrai canard at Σ_{fold} as $\varepsilon \rightarrow 0$, are linearly independent. It subsequently also follows that the periodic orbit, being the transverse intersection of an attracting slow manifold and a repelling one, is of saddle-type. \square

Figure 12(b) shows numerically that the discontinuous model (4) satisfies the assumptions of Proposition 6.6. This supports the existence of the branch Π_ε^c in the regularized model for ε sufficiently small. Because of the symmetry, the branch Π_ε^c has two canard segments for each period. A *canard explosion* may appear when a family of periodic orbits interacts with a canard. The explosion is defined as the transition from a small oscillation to a relaxation oscillation for an exponentially small variation in the parameter [41]. However, system (10) has no canard explosion: Figure 11(a) shows that the maximum amplitude of the oscillations does not increase with the continuation from Π_ε^l to Π_ε^c . The effect of the canard lies instead in the explosion of one of the Floquet multipliers, as previously stated in Proposition 6.6 and observed numerically in AUTO. The saddle stability of the family Π_ε^c implies that the periodic orbits of Π_ε^c are always repelling, even with a time inversion. Hence, these periodic

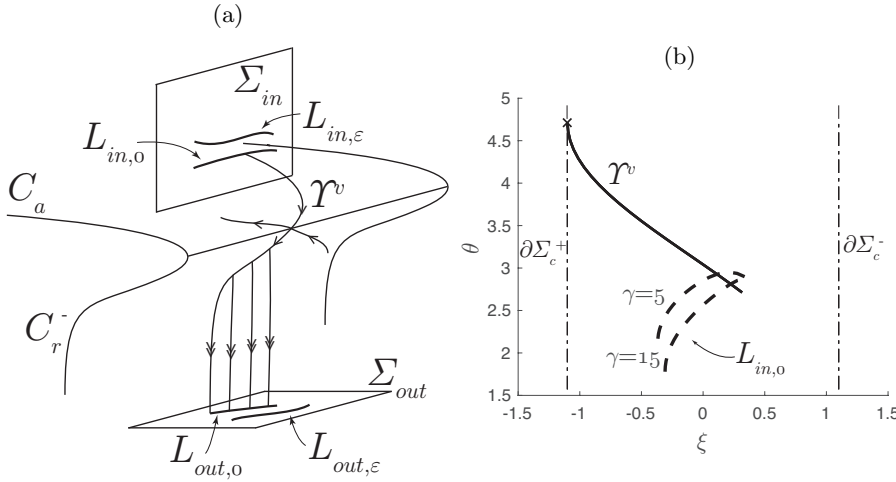


Fig. 12 (a) Construction of the cross-sections $\Sigma_{in,out}$. (b) Numerical simulation showing that $R(L_{out,0})$ (dashed line) is transversal to γ^v (solid line) for $\varepsilon = 0$ and $\gamma = \{5, 15\}$. The visible tangency is marked with x . The dashed-dotted lines are $\partial\Sigma_c^\pm$.

orbits are not visible in standard simulations. However, their stable manifolds act as separatrices between the basins of attraction of the slip-stick periodic orbits and the pure stick orbits described in Proposition 5.4. It would be interesting to design an experiment, with very high precision in the initial conditions, in which the effects of the canard are measurable. If canard solutions appear, then this would support the validity of the stiction model and its regularization.

PROPOSITION 6.7. *The branch Π_ε^c is bounded above by $\gamma = 1/\sqrt{\varepsilon\delta}$ for $0 < \varepsilon \ll 1$.*

Proof. Differentiate $\xi(x, \theta) = \gamma^2 x + \sin(\theta)$ with respect to time, and rewrite the slow problem (13) in the (ξ, \hat{y}, θ) variables

$$\begin{aligned} \xi' &= \gamma^2 \varepsilon \hat{y} + \cos \theta, \\ \varepsilon \hat{y}' &= -\xi - \mu_d \phi(\hat{y}), \\ \theta' &= 1. \end{aligned}$$

If $\gamma^2 = O(1/\varepsilon)$, it makes sense to introduce the rescaling $\Gamma := \gamma^2 \varepsilon$, so that the slow problem becomes

$$\begin{aligned} \xi' &= \Gamma \hat{y} + \cos \theta, \\ \varepsilon \hat{y}' &= -\xi - \mu_d \phi(\hat{y}), \\ \theta' &= 1. \end{aligned}$$

This system again has a multiple time scale with critical manifold (17). Its reduced problem in time \hat{t} is

$$\begin{aligned} \dot{\hat{y}} &= -\Gamma \hat{y} - \cos \theta, \\ (28) \quad \dot{\theta} &= \mu_d \phi'(\hat{y}). \end{aligned}$$

Notice that (28) differs from the desingularized problem (24) only in the term $\Gamma \hat{y}$ in the \hat{y} dynamics. The fixed points of (28) exist if $|\Gamma \delta| \leq 1$, and they have coordinates

$\hat{y} = \pm\delta$, $\cos\theta = \mp\Gamma\delta$. The comparison of system (28) with the desingularized problem (24) shows that the fixed points have shifted along the θ -direction. In particular, the saddles have moved backward while the centers have moved forward. Furthermore, the centers have become stable foci. For increasing values of Γ the stable foci turn into stable nodes. When $|\Gamma\delta| = 1$, pairs of saddles and nodes collide and disappear through a saddle-node bifurcation of type I [43, Lemma 8.5.7]. Beyond this value, canard solutions cease to exist. Such a condition is equivalent to $\gamma = 1/\sqrt{\varepsilon\delta}$. \square

The bound $\gamma = 1/\sqrt{\varepsilon\delta}$, which is highlighted in Figure 11(b), is larger than the value of γ for which the family Π_ε^c folds. In particular, at the turning point, the folded foci have not yet turned into folded nodes. Thus, the collision of the folded saddles with the folded foci is not a direct cause of the saddle-node bifurcation of Π_ε^c , but gives only an upper bound for the existence of the family. Notice also that when the folded nodes appear, there might exist further periodic orbits that exit the slow regime through the canard associated to the stable nodes.

Furthermore, the orbits of Π_ε^c interact with the folded saddle only, and they do not interact with the other points of \hat{I}^\pm . The regularized problem (10) may have other families of periodic orbits that interact with \hat{I}^\pm , for example, a family of pure slip periodic orbits that reaches \hat{I}^\pm from a fast fiber and then jumps off through a canard-like solution. However, this family would also turn unstable when passing sufficiently close to the canards because of the high sensitivity to the initial conditions around \mathcal{F}^\pm . In particular, an explosion in the Floquet multipliers is again expected because of Proposition 6.6.

7. Conclusions. Nonuniqueness of solutions is intrinsic in nonsmooth modeling [28]. On a fundamental level, nonuniqueness is even problematic in numerical simulations, where a choice is required and “valid solutions” might therefore be discarded. In this paper, we have shed further light on nonuniqueness and developed a new terminology for “valid solutions” through the analysis of a simple piecewise-smooth model of a forced mass-spring system subject to stiction friction.

Stiction is a widely used piecewise-smooth formulation of the friction force because of its simplicity. However, as demonstrated, this friction law has issues of nonuniqueness at the onset of slip. A regularization of the model resolves the nonuniqueness and we have found a repelling slow manifold that separates forward sticking and forward slipping solutions. Around the slow manifold there is a high sensitivity to the initial conditions. Some trajectories remain close to this slow manifold for some time before being repelled. These trajectories, which mathematically are known as canards, have the physical interpretation of delaying the slip onset when the external forces have equaled the maximum static friction force at stick. This result could potentially be verified experimentally, thus furthering the understanding of friction-related phenomena. Indeed, the appearance of the canard solutions is a feature of stiction friction rather than the specific friction oscillator model. For example, the addition of a damping term on the friction oscillator or the problem of a mass on an oscillating belt would give rise to similar canard solutions. Moreover, these canards appear generically within the class of regularization functions that we consider. In fact, the system is qualitatively independent of the regularization, which is an important observation.

The canard solutions of the regularized systems can be interpreted, in the discontinuous model, as Carathéodory trajectories that allow the slip onset at points inside the sticking region. These Carathéodory orbits are identified by being backwards transverse to the lines of nonuniqueness.

The paper has also shown that the regularized system has a family of periodic orbits Π_ε interacting with the folded saddles. The orbits with canard $\Pi_\varepsilon^c \subset \Pi_\varepsilon$ have a saddle stability, and we showed, in Proposition 6.6, in an abstract setting, that this relates to a canard-like explosion of the Floquet multipliers $O(e^{\pm c\varepsilon^{-1}})$. Furthermore, we observed that the family Π_ε^c connects, in the rigid body limit, the two families of slip-stick periodic orbits $\Pi_0^{l,r}$ that are otherwise disconnected for the discontinuous problem. We speculate that the connectedness of the cycles are related to a tangency of the image of the return map R with the canard (see Figure 12) and that it might be possible to do a more thorough analysis of the rigid-body limit by doing a proper scaling and blowup analysis (see, e.g., [29, 38]). We also speculate that this tangency is associated with the onset of chaos through a horseshoe (see also [22, 23] for related work on chaos in the forced van der Pol), but we leave this to future work. We complete the paper by emphasizing that our approach is general enough to apply to systems of increased complexity (e.g., higher dimension).

REFERENCES

- [1] A. AKAY, *Acoustics of friction*, J. Acoust. Soc. Amer., 111 (2002), pp. 1525–1548, <https://doi.org/10.1121/1.1456514>. (Cited on p. 870)
- [2] U. ANDREAS AND P. CASINI, *Dynamics of friction oscillators excited by a moving base and/or driving force*, J. Sound Vibration, 245 (2001), pp. 685–699, <https://doi.org/10.1006/jsvi.2000.3555>. (Cited on pp. 887, 889)
- [3] E. BENOÎT, J. F. CALLOT, F. DIENER, AND M. DIENER, *Chasse au canard*, Collect. Math., 32 (1981), pp. 37–119. (Cited on p. 884)
- [4] E. BOSSOLINI, E., M. BRØNS, AND K. U. KRISTIANSEN, *Singular limit analysis of a model for earthquake faulting*, Nonlinearity, 30 (2017), pp. 2805–2834, <https://doi.org/10.1088/1361-6544/aa712e>. (Cited on p. 870)
- [5] P. A. BLIMAN AND M. SORINE, *Easy-to-use realistic dry friction models for automatic control*, in Proceedings of the 3rd European Control Conference, 1995, pp. 3778–3794. (Cited on p. 878)
- [6] C. CANTONI, R. CESARINI, G. MASTINU, G. ROCCA, AND R. SICIGLIANO, *Brake comfort—A review*, Vehicle Syst. Dyn., 47 (2009), pp. 901–947, <https://doi.org/10.1080/00423110903100432>. (Cited on p. 870)
- [7] P. CARTER, E. KNOBLOCH, AND M. WECHSELBERGER, *Transonic canards and stellar wind*, Nonlinearity, 30 (2017), pp. 1006–1033, <https://doi.org/10.1088/1361-6544/aa5743>. (Cited on p. 885)
- [8] J. CORTES, *Discontinuous dynamical systems*, IEEE Control Syst., 28 (2008), pp. 36–73, <https://doi.org/10.1109/MCS.2008.919306>. (Cited on p. 877)
- [9] G. CSERNÁK AND G. STÉPÁN, *On the periodic response of a harmonically excited dry friction oscillator*, J. Sound Vibration, 295 (2006), pp. 649–658, <https://doi.org/10.1016/j.jsv.2006.01.030>. (Cited on pp. 871, 876, 887, 889)
- [10] G. CSERNÁK, G. STÉPÁN, AND S. W. SHAW, *Sub-harmonic resonant solutions of a harmonically excited dry friction oscillator*, Nonlinear Dynam., 50 (2007), pp. 93–109, <https://doi.org/10.1007/s11071-006-9145-6>. (Cited on p. 877)
- [11] E. J. DEODEL, *Lecture notes on numerical analysis of nonlinear equations*, in Numerical Continuation Methods for Dynamical Systems, B. Krauskopf, H. M. Osinga, and J. Galán-Vioque, eds., Springer, Dordrecht, 2016, pp. 1–49, https://doi.org/10.1007/978-1-4020-6356-5_1. (Cited on p. 889)
- [12] M. DI BERNARDO, C. BUDD, A. R. CHAMPNEYS, AND P. KOWALCZYK, *Piecewise-Smooth Dynamical Systems*, Springer-Verlag, London, 2008, <https://doi.org/10.1007/978-1-84628-708-4>. (Cited on pp. 871, 874, 875, 876)
- [13] J. H. DIETERICH, *Time-dependent friction and mechanics of stick-slip*, Pure Appl. Geophys., 116 (1978), pp. 790–806, <https://doi.org/10.1029/JB084iB05p02161>. (Cited on p. 870)
- [14] J. H. DIETERICH, *Modeling of rock friction. 1. Experimental results and constitute equations*, J. Geophys. Res., 84 (1979), pp. 2161–2168, <https://doi.org/10.1029/JB084iB05p02161>. (Cited on p. 870)
- [15] F. DUMORTIER AND R. ROUSSARIE, *Canard cycles and center manifolds*, Mem. Amer. Math. Soc., 121 (1996), 577, <https://doi.org/10.1090/memo/0577>. (Cited on pp. 871, 884)

- [16] B. FEENY, A. GURAN, N. HINRICHES, AND K. POPP, *A historical review on dry friction and stick-slip phenomena*, Appl. Mech. Rev., 51 (1998), pp. 321–341, <https://doi.org/10.1115/1.3099008>. (Cited on p. 870)
- [17] N. FENICHEL, *Asymptotic stability with rate conditions for dynamical systems*, Bull. Amer. Math. Soc., 80 (1974), pp. 346–349. (Cited on pp. 871, 881)
- [18] N. FENICHEL, *Geometric singular perturbation theory for ordinary differential equations*, J. Differential Equations, 31 (1979), pp. 53–98, [https://doi.org/10.1016/0022-0396\(79\)90152-9](https://doi.org/10.1016/0022-0396(79)90152-9). (Cited on pp. 871, 881)
- [19] A. F. FILIPPOV, *Differential Equations with Discontinuous Righthand Sides*, Springer, Dordrecht, 1988. (Cited on pp. 871, 874, 876, 877)
- [20] U. GALVANETTO AND S. R. BISHOP, *Dynamics of a simple damped oscillator undergoing stick-slip vibrations*, Meccanica, 34 (1999), pp. 337–347, <https://doi.org/10.1023/A:1004741715733>. (Cited on p. 887)
- [21] M. GUARDIA, S. J. HOGAN, AND T. M. SEARA, *An analytical approach to codimension-2 sliding bifurcations in the dry-friction oscillator*, SIAM J. Appl. Dyn. Syst., 9 (2010), pp. 769–798, <https://doi.org/10.1137/090766826>. (Cited on pp. 874, 877)
- [22] J. GUCKENHEIMER, K. HOFFMAN, AND W. WECKESSER, *Bifurcations of relaxation oscillations near folded saddles*, Internat. J. Bifur. Chaos Appl. Sci. Engrg., 15 (2005), pp. 3411–3421, <https://doi.org/10.1142/S0218127405014131>. (Cited on pp. 885, 894)
- [23] R. HAIDUC, *Horseshoes in the forced van der Pol system*, Nonlinearity, 22 (2009), pp. 213–237, <https://doi.org/10.1088/0951-7715/22/1/011>. (Cited on p. 894)
- [24] M. A. HECKL AND I. D. ABRAHAMS, *Curve squeal of train wheels, part 1: Mathematical model for its generation*, J. Sound Vibration, 229 (2000), pp. 669–693, <https://doi.org/10.1006/jsvi.1999.2510>. (Cited on p. 870)
- [25] N. HINRICHES, M. OESTREICH, AND K. POPP, *Experimental and numerical investigation of a friction oscillator*, ASME DE, 90 (1996), pp. 57–62. (Cited on p. 870)
- [26] N. HINRICHES, M. OESTREICH, AND K. POPP, *On the modelling of friction oscillators*, J. Sound Vibration, 216 (1998), pp. 435–459, <https://doi.org/10.1006/jsvi.1998.1736>. (Cited on pp. 871, 887)
- [27] S. J. HOGAN, AND K. U. KRISTIANSEN, *On the regularization of impact without collision: The Painlevé paradox and compliance*, Proc. Math. Phys. Eng. Sci., 473 (2017), art. 20160773, <https://doi.org/10.1098/rspa.2016.0773>. (Cited on p. 870)
- [28] M. R. JEFFREY, *Hidden Dynamics: The Mathematics of Switches, Decisions and Other Discontinuous Behaviour*, Springer, Berlin, 2018, <https://doi.org/10.1007/978-3-030-02107-8>. (Cited on p. 893)
- [29] S. JELBART, K. ULDALL KRISTIANSEN, P. SZMOLYAN, AND M. WECHSELBERGER, *Singularly Perturbed Oscillators with Exponential Nonlinearities*, preprint, <https://arxiv.org/abs/1912.11769>, 2020. (Cited on pp. 870, 871, 894)
- [30] S. JELBART, K. ULDALL KRISTIANSEN, AND M. WECHSELBERGER, *Singularly Perturbed Boundary-Focus Bifurcations*, preprint, <https://arxiv.org/abs/2006.06087>, 2020. (Cited on pp. 870, 871)
- [31] C. K. R. T. JONES, *Geometric singular perturbation theory*, in Dynamical Systems, R. Johnson, ed., Lecture Notes in Math. 1609, Springer, Berlin, Heidelberg, 1995, pp. 44–118, <https://doi.org/10.1007/BFb0095239>. (Cited on pp. 871, 880)
- [32] I. KOSIUK, AND P. SZMOLYAN, *Geometric analysis of the Goldbeter minimal model for the embryonic cell cycle*, J. Math. Biol., 72 (2016), pp. 1337–1368, <https://doi.org/10.1007/s00285-015-0905-0> (Cited on p. 871)
- [33] P. KOWALCZYK AND P. T. PIHOINEN, *Two-parameter sliding bifurcations of periodic solutions in a dry-friction oscillator*, Phys. D, 237 (2008), pp. 1053–1073, <https://doi.org/10.1016/j.physd.2007.12.007>. (Cited on p. 877)
- [34] K. U. KRISTIANSEN, *Blowup for flat slow manifolds*, Nonlinearity, 30 (2017), pp. 2138–2184, <http://stacks.iop.org/0951-7715/30/i=5/a=2138>. (Cited on pp. 881, 882)
- [35] K. U. KRISTIANSEN AND S. J. HOGAN, *On the use of blowup to study regularizations of singularities of piecewise smooth dynamical systems in \mathbb{R}^3* , SIAM J. Appl. Dyn. Syst., 14 (2015), pp. 382–422, <https://doi.org/10.1137/140980995>. (Cited on pp. 870, 871, 882)
- [36] K. U. KRISTIANSEN AND S. J. HOGAN, *Resolution of the piecewise smooth visible-invisible two-fold singularity in \mathbb{R}^3 using regularization and blowup*, J. Nonlinear Sci., 29 (2018), pp. 723–787, <https://doi.org/10.1007/s00332-018-9502-x>. (Cited on pp. 870, 871, 881, 882)
- [37] K. U. KRISTIANSEN AND S. J. HOGAN, *Le Canard de Painlevé*, SIAM J. Appl. Dyn. Syst., 17 (2018), pp. 859–908, <https://doi.org/10.1137/17M1122256>. (Cited on p. 870)
- [38] K. U. KRISTIANSEN AND P. SZMOLYAN, *Relaxation Oscillations in Substrate-Depletion Oscillators Close to the Nonsmooth Limit*, preprint, <https://arxiv.org/abs/1909.11746v2>, 2019. (Cited on pp. 870, 871, 881, 882, 894)

- [39] K. U. KRISTIANSEN, *A new type of relaxation oscillation in a model with rate-and-state friction*, Nonlinearity, 33 (2020), pp. 2960–3037, <https://doi.org/10.1088/1361-6544/ab73cf>. (Cited on p. 870)
- [40] K. U. KRISTIANSEN, *The regularized visible fold revisited*, J. Nonlinear Sci., (2020), <https://doi.org/10.1007/s00332-020-09627-8>. (Cited on pp. 870, 871, 881, 882)
- [41] M. KRUPA AND P. SZMOLYAN, *Relaxation oscillation and canard explosion*, J. Differential Equations, 174 (2001), pp. 312–368, <https://doi.org/10.1006/jdeq.2000.3929>. (Cited on pp. 871, 891)
- [42] M. KRUPA AND M. WECHSELBERGER, *Local analysis near a folded saddle-node singularity*, J. Differential Equations, 248 (2010), pp. 2841–2888, <https://doi.org/10.1016/j.jde.2010.02.006>. (Cited on p. 885)
- [43] C. KUEHN, *Multiple Time Scale Dynamics*, Springer, Cham, 2015, <https://doi.org/10.1007/978-3-319-12316-5>. (Cited on pp. 880, 885, 893)
- [44] G. LICSÓK AND G. CSERNÁK, *On the chaotic behaviour of a simple dry-friction oscillator*, Math. Comput. Simul., 95 (2014), pp. 55–62, <https://doi.org/10.1016/j.matcom.2013.03.002>. (Cited on p. 871)
- [45] J. LLIBRE, P. R. DA SILVA, AND M. A. TEIXEIRA, *Sliding vector fields via slow-fast systems*, Bull. Belg. Math. Soc. Simon Stevin, 15 (2008), pp. 851–869. (Cited on pp. 870, 871, 882)
- [46] J. D. MEISS, *Differential Dynamical Systems*, Math. Model. Comput. 14, SIAM, Philadelphia, 2007, <https://doi.org/10.1137/1.9780898718232>. (Cited on pp. 871, 887)
- [47] M. NAKATANI, *Conceptual and physical clarification of rate and state friction: Frictional sliding as a thermally activated rheology*, J. Geophys. Res. Solid Earth, 106 (2001), pp. 13347–13380, <https://doi.org/10.1029/2000JB900453>. (Cited on p. 870)
- [48] M. OESTREICH, N. HINRICHES, AND K. POPP, *Bifurcation and stability analysis for a non-smooth friction oscillator*, Arch. Appl. Mech., 66 (1996), pp. 301–314, <https://doi.org/10.1007/BF00795247>. (Cited on pp. 887, 889)
- [49] H. OLSSON AND K. J. ÅSTRÖM, *Friction generated limit cycles*, IEEE Trans. Control Syst. Technol., 9 (2002), pp. 629–636, <https://doi.org/10.1109/87.930974>. (Cited on pp. 870, 871, 887)
- [50] H. OLSSON, K. J. ÅSTRÖM, C. CANUDAS DE WIT, M. GÄFVERT, AND P. LISCHINSKY, *Friction models and friction compensation*, Eur. J. Control, 4 (1998), pp. 176–195, [https://doi.org/10.1016/s0947-3580\(98\)70113-x](https://doi.org/10.1016/s0947-3580(98)70113-x). (Cited on pp. 870, 878)
- [51] E. PENNESTRÌ, V. ROSSI, P. SALVINI, AND P. P. VALENTINI, *Review and comparison of dry friction force models*, Nonlinear Dynam., 83 (2016), pp. 1785–1801, <https://doi.org/10.1007/s11071-015-2485-3>. (Cited on p. 870)
- [52] K. POPP AND P. STELTER, *Stick-slip vibrations and chaos*, Philos. Trans. Roy. Soc. London Ser. A, 332 (1990), pp. 89–105, <https://doi.org/10.1098/rsta.1990.0102>. (Cited on pp. 871, 887)
- [53] T. K. PRATT AND R. WILLIAMS, *Non-linear analysis of stick/slip motion*, J. Sound Vibration, 74 (1981), pp. 531–542, [https://doi.org/10.1016/0022-460X\(81\)90417-X](https://doi.org/10.1016/0022-460X(81)90417-X). (Cited on p. 870)
- [54] T. PUTELAT, J. H. P. DAWES, AND A. R. CHAMPNEYS, *A phase-plane analysis of localized frictional waves*, Proc. A, 473 (2017), art. 20160606, <https://doi.org/10.1098/rspa.2016.0606>. (Cited on p. 870)
- [55] T. PUTELAT, J. H. P. DAWES, AND J. R. WILLIS, *Regimes of frictional sliding of a spring-block system*, J. Mech. Phys. Solids, 58 (2010), pp. 27–53, <https://doi.org/10.1016/j.jmps.2009.09.001>. (Cited on p. 870)
- [56] E. RABINOWICZ, *The nature of the static and kinetic coefficients of friction*, J. Appl. Phys., 22 (1951), pp. 1373–1379, <https://doi.org/10.1063/1.1699869>. (Cited on pp. 870, 872)
- [57] A. RUINA, *Slip instability and state variable friction laws*, J. Geophys. Res., 88 (1983), pp. 359–370, <https://doi.org/10.1029/JB088iB12p10359>. (Cited on p. 870)
- [58] S. SCHECTER AND P. SZMOLYAN, *Composite waves in the Dafermos regularization*, J. Dyn. Differential Equations, 16 (2004), pp. 847–867, <https://doi.org/10.1007/s10884-004-6698-2>. (Cited on p. 870)
- [59] S. W. SHAW, *On the dynamic response of a system with dry friction*, J. Sound Vibration, 108 (1986), pp. 305–325, [https://doi.org/10.1016/S0022-460X\(86\)80058-X](https://doi.org/10.1016/S0022-460X(86)80058-X). (Cited on pp. 871, 876, 887)
- [60] J. SOTOMAYOR AND M. A. TEIXEIRA, *Regularization of discontinuous vector fields*, in International Conference on Differential Equations (Lisboa, 1995), World Scientific, River Edge, NJ, 1996, pp. 207–223. (Cited on pp. 871, 882)
- [61] P. SZMOLYAN AND M. WECHSELBERGER, *Canards in \mathbb{R}^3* , J. Differential Equations, 177 (2001), pp. 419–453, <https://doi.org/10.1006/jdeq.2001.4001>. (Cited on pp. 871, 885, 886, 891)

- [62] P. SZMOLYAN AND M. WECHSELBERGER, *Relaxation oscillations in \mathbb{R}^3* , J. Differential Equations, 200 (2004), pp. 69–104, <https://doi.org/10.1016/j.jde.2003.09.010>. (Cited on pp. 883, 889)
- [63] A. N. TIKHONOV AND V. Y. ARSENIN, *Solutions of Ill-Posed Problems*, V. H. Winston & Sons, Washington, D.C., 1977. (Cited on p. 870)
- [64] M. A. TEIXEIRA, *Generic bifurcation of sliding vector-fields*, J. Math. Anal. Appl., 176 (1993), pp. 436–457, <https://doi.org/10.1006/jmaa.1993.1226>. (Cited on p. 875)
- [65] T. VO AND M. WECHSELBERGER, *Canards of folded saddle-node type I*, SIAM J. Math. Anal., 47 (2015), pp. 3235–3283, <https://doi.org/10.1137/140965818>. (Cited on p. 885)
- [66] S. WIECZOREK, P. ASHWIN, C. M. LUKE, AND P. M. COX, *Excitability in ramped systems: The compost-bomb instability*, Proc. R. Soc. Lond. Ser. A Math. Phys. Eng. Sci., 467 (2011), pp. 1243–1269, <https://doi.org/10.1098/rspa.2010.0485>. (Cited on p. 885)
- [67] J. WOJEWODA, A. STEFAŃSKI, M. WIERCIGROCH, AND T. KAPITANIAK, *Hysteretic effects of dry friction: Modelling and experimental studies*, Philos. Trans. R. Soc. Lond. Ser. A Math. Phys. Eng. Sci., 366 (2008), pp. 747–765, <https://doi.org/10.1098/rsta.2007.2125>. (Cited on p. 870)
- [68] J. WOODHOUSE, T. PUTELAT, AND A. MCKAY, *Are there reliable constitutive laws for dynamic friction?*, Philos. Trans. R. Soc. Lond. Ser. A Math. Phys. Eng. Sci., 373 (2015), art. 20140401, <https://doi.org/10.1098/rsta.2014.0401>. (Cited on p. 870)